Pergamon

Int. J. Solids Structures Vol. 32, No. 11, pp. 1607–1641, 1995
Elsevier Science Ltd
Printed in Great Britain
0020–7683/95 $9.50 + .00

0020–7683(94)00195–2

A FULLY COUPLED ELASTO-VISCO-PLASTIC DAMAGE THEORY FOR ANISOTROPIC MATERIALS

Y. Y. ZHU†
Materials Process Modeling Group, Metals and Ceramics Division, Oak Ridge National Laboratory, TN 37831-6140, U.S.A.

and

S. CESCOTTO
Département MSM, Université de Liège, B-4000, Belgium

(*Received* 19 *July* 1993; *in revised form* 10 *August* 1994)

Abstract—In this paper, the development of an energy-based anisotropic damage model at finite strains for ductile fracture is described. The constitutive model is developed within the general framework of continuum thermodynamics for irreversible processes by identifying a proper set of internal variables together with their associated generalized forces. Three major anisotropies are considered, including anisotropic elasticity, anisotropic plasticity and anisotropic damage. The physical implications, mathematical restrictions, and numerical implementations, as well as practical applications are discussed in some detail. Attention is focused on the development of a new damage characteristic tensor which is based on the hypothesis of damage energy equivalence and provides a good physical representation of damage evolution. An approach is also presented to account for microcrack opening and closing. A viscoplastic regularization algorithm is proposed to take into account the strain rate effect and to improve numerical stability. The numerical implementation is described in detail. In particular, a new and simple two-step operator split algorithm (elastic predictor and coupled plastic-damage corrector) with subincrements is developed which can efficiently integrate fully coupled elastoplastic damage constitutive relations. Numerical results are presented for sheet forming processes. Good agreement with some theoretical and experimental results is also obtained.

1. INTRODUCTION

It is well-known that most structural materials exhibit some degree of anisotropy. Some materials, such as fibrous composites, polymers and timber are naturally anisotropic. In sheet forming in particular, the effect of anisotropy on the deformation characteristics may be appreciable and important, because the sheets are usually cold-rolled and possess different properties in rolling and transverse directions (Kobayashi *et al.*, 1989).

Recent experimental evidence indicates that structural failures are often associated with the development of anisotropic material damage even if the initial material properties are isotropic. In fact, anisotropy of damage is supported by microscopic observations: microvoids or microcracks extend more on planes normal to the maximum principal stress axis. The importance of the directional nature of material damage in controlling final rupture becomes more pronounced under non-proportional service loadings (Chaboche, 1987). An analysis without taking into account the damage-induced material anisotropy may therefore yield questionable results. This has prompted several researches to investigate the general case of anisotropic damage.

Instead of using scalar damage variables for isotropic damage models (Lemaitre, 1985), a number of anisotropic damage models have been developed incorporating separately vectors and tensors of second order or higher ranks as state variables characterizing anisotropic damage.

†Formerly a doctoral student at Département MSM, Université de Liège, Belgium.

One of the first works was developed by Cordebois and Sidoroff (1979 and 1982) and Cordebois (1983). They have proposed an anisotropic ductile plastic damage model based on elastic energy equivalence. Later, Lee *et al.* (1985) used this model to predict the forming limits of an anisotropic metal plate with a new damage criterion for deformation instability. However, in this model, the damage effect tensor $\underline{M}$ for the effective stress equation and the damage characteristic tensor $\underline{J}$ developed for the damage evolution rule were limited to a few special cases with *a priori* knowledge of principal stress/strain directions. For solutions of most practical engineering problems, this requirement is too restrictive.

The modification which removes this restriction was proposed by Chow and Wang (1987, 1988, 1991) by introducing a generalized damage effect tensor $\underline{M}$ and appropriate coordinate transformation for the tensor. Recently, Voyiadjis and Katton (1990, 1992) have extended this version to large strain analysis. However, the criterion of damage evolution is based on "effective damage stress" in the above works. The physical significance is not clear and may violate the thermodynamic rules, because the thermodynamic conjugate force of the damage tensor $\underline{D}$ is assumed to be the stress tensor $\underline{\sigma}$.

In order to avoid this drawback, Chow and Lu (1989a, b) and Lu and Chow (1990) returned to use the energy based criterion of damage evolution which was originally proposed by Cordebois and Sidoroff (1982, 1983), but with a new damage characteristic tensor $\underline{J}$. Identification of $\underline{J}$ is simple enough (it involves only one unknown parameter) to be determined from a standard tensile test. However, this new version of the anisotropic damage model is only suited to the case when the initial material properties are isotropic.

Another anisotropic damage model proposed by Simo and Ju (1987a, b) and Ju (1989a, b, 1990b) should be mentioned. In this model, the free energy involved in the plastic flow and damaging processes is coupled explicitly. However it is difficult to express the criterion of damage evolution with a unified form because uncoupled treatment of damage and plasticity is not an easy task.

In this paper, the energy based anisotropic damage model proposed originally by Cordebois and Sidoroff (1979, 1982) and Cordebois (1983) is extended with some special considerations:

(1) three major anisotropies are taken into account, including: anisotropic elasticity, anisotropic plasticity and anisotropic damage;

(2) the generalized damage effect tensor $\underline{M}$ proposed by Chow and Wang, 1987 is used;

(3) a generalized coordinate transformation between the material principal axes and reference coordinate axes is suggested;

(4) a new damage characteristic tensor $\underline{J}$ based on the hypothesis of damage energy equivalence is proposed;

(5) microcrack opening and closing mechanism is considered thanks to different effects of tensile and compressive states;

(6) the viscous regularization of the rate-independent damage model to take into account the effect of strain rate and to improve the numerical convergence is made;

(7) finally, an effective computational integration algorithm with two step split operators is proposed.

2. CHARACTERIZATION OF ANISOTROPIC DAMAGE

2.1. *Effective stress and damage effect tensor* $\underline{\mathrm{M}}(\underline{\mathrm{D}})$

One basic hypothesis in most isotropic and anisotropic models of continuum damage mechanics is that, neglecting the details of microscopic damage growth, damage can be viewed as a macroscopic state variable which affects the average microscopic damage growth in the sense of "effective stress". This basic hypothesis of effective stress can be stated this way: there exists a "damage effect tensor" $\underline{M}(\underline{D})$ applied to the stress tensor $\underline{\sigma}$ which defines the effective stress tensor $\underline{\bar{\sigma}}$ (Chaboche, 1981, 1984), that is:

$$\bar{\underline{\sigma}} = \underline{M}(\underline{D})\,\underline{\sigma} \tag{1}$$

where the damage effect tensor $\underline{M}(\underline{D})$ is a second-order or fourth-order tensor depending on the damage tensor $\underline{D}$. Note that four fundamental variables of continuum damage mechanics have been introduced in the foregoing hypothesis, i.e. the damage tensor $\underline{D}$, the damage effect tensor $\underline{M}(\underline{D})$, the effective stress tensor $\bar{\underline{\sigma}}$ and effective strain tensor $\bar{\underline{\varepsilon}}$.

Damage induced material anisotropy may be characterized by a symmetric second-order tensor $\underline{D}$. Because of its mathematical simplicity, $\underline{D}$ has been used extensively to study various aspects of damage problems including elasticity (Cordebois and Sidoroff 1979; Chow and Wang 1987; Valliappan *et al.* 1990), elastoplasticity (Cordebois and Sidoroff 1982; Cordebois, 1983; Lee *et al.*, 1985) and elasto-visco-plasticity (Saaouni *et al.*, 1989). Perhaps the most attractive property of $\underline{D}$ is that it always possesses three orthogonal principal directions and the corresponding principal values (Lu and Chow 1990).

There is no uniquely defined mathematical formulation of $\underline{M}(\underline{D})$ and indeed various formulations have been proposed (Chow and Lu, 1989a). One of the simplest forms is to introduce material damage in the stress tensor principal directions only (Cordebois and Sidoroff, 1979, Lee *et al.*, 1985):

$$[\bar{\sigma}_1\ \bar{\sigma}_2 \bar{\sigma}_3]^T = \underline{M}[\sigma_1\ \sigma_2\ \sigma_3]^T \tag{2a}$$

with the second order of damage effect tensor:

$$\underline{M}(\underline{D}) = \begin{bmatrix} \dfrac{1}{1-D_1} & 0 & 0 \\ 0 & \dfrac{1}{1-D_2} & 0 \\ 0 & 0 & \dfrac{1}{1-D_3} \end{bmatrix} \tag{2b}$$

where D_1, D_2 and D_3 are damage variables in their principal axes. However, when the directions of the principal stresses are unknown, the damage effect tensor (2b) must be suitably modified. One obvious criterion for developing such a generalized form of the damage effect tensor is that it should reduce to a scalar for isotropic damage. This reduction should be made possible not only in a principal coordinate system but also in any coordinate system.

One formulation which satisfies the above criterion was proposed by Chow and Wang (1987), in the principal coordinate system of damage as:

$$[\bar{\sigma}_{11}\ \bar{\sigma}_{22}\ \bar{\sigma}_{33}\ \bar{\sigma}_{23}\ \bar{\sigma}_{31}\ \bar{\sigma}_{12}]^T = \underline{M}[\sigma_{11}\ \sigma_{22}\ \sigma_{33}\ \sigma_{23}\ \sigma_{31}\ \sigma_{12}]^T \tag{3a}$$

with the fourth rank symmetric tensor:

$$\underline{M} = \text{diag}\left[\frac{1}{1-D_1}\ \frac{1}{1-D_2}\ \frac{1}{1-D_3}\ \frac{1}{\sqrt{(1-D_2)(1-D_3)}}\ \frac{1}{\sqrt{(1-D_3)(1-D_1)}}\ \frac{1}{\sqrt{(1-D_1)(1-D_2)}}\right]. \tag{3b}$$

It is obvious that (2) is a particular case of (3) which can be readily reduced to a scalar for isotropic damage when $D_1 = D_2 = D_3 = D$. Because the generalized damage effect tensor $M(D)$ in eqn (3) can be applied to solve common structural engineering problems (Jubran and Cofter 1991), it will be used to derive the constitutive equations of the present anisotropic damage model.

2.2. *Hypothesis of energy equivalence*

Instead of the conventional postulate of strain or stress equivalence which has rather limited ability in the establishment of constitutive equations of materials suffering from progressive deterioration especially when anisotropic damage is involved, an hypothesis of energy equivalence was proposed by Cordebois and Sidoroff (1979, 1982) which states that the complementary elastic energy for a damaged material has the same form as that of a fictitious undamaged material except that the stress is replaced by the effective stress in the energy formulation. Mathematically,

$$W_e(\underline{\sigma}, \underline{D}) = W_e(\underline{\bar{\sigma}}, \underline{D}) \tag{4a}$$

or

$$\tfrac{1}{2}\underline{\bar{\sigma}}^T \underline{C}_e^{-1} \underline{\bar{\sigma}} = \tfrac{1}{2}\underline{\sigma}^T \underline{\bar{C}}_e^{-1} \underline{\sigma} \tag{4b}$$

where $\underline{C}_e$ and $\underline{\bar{C}}_e$ are the virgin and damaged elastic material stiffness tensors respectively. By recalling (1), it can be easily proved that:

$$\underline{\bar{C}}_e^{-1} = \underline{M}(\underline{D})\, \underline{C}_e^{-1}\, \underline{M}(\underline{D}) \tag{5}$$

and according to the hypothesis of energy equivalence the effective elastic strain vector is

$$\underline{\bar{\varepsilon}}_e = \underline{M}^{-1}\, \underline{\varepsilon}_e \tag{6}$$

where:

$$\underline{M}^{-1} = \text{diag}$$

$$[1-D_1\ 1-D_2\ 1-D_3\ \sqrt{(1-D_2)(1-D_3)}\ \sqrt{(1-D_3)(1-D_1)}\ \sqrt{(1-D_1)(1-D_2)}]. \tag{7}$$

3. GENERAL THERMODYNAMIC ANALYSIS

3.1. *State variables*

The internal variables to be used in the thermodynamic analysis are listed, together with their associated thermodynamic forces, in Table 1. The general structure of the constitutive equations is furnished by the well-established thermodynamic theory of irreversible processes with such state variables. Hereafter, isothermal condition is assumed.

3.2. *Thermodynamic potential*

As it has been indicated in Lemaitre (1985), uncoupled plasticity and elasticity is assumed such that the elastic properties depend only on damage variables and not on the dislocation density α. For practical purposes, another hypothesis is introduced: energies involved in plastic flow and damage processes, dissipated by heat or stored in the material due to hardening, are independent. Consequently, in the present model, the Helmholtz free energy takes the following form (Lu and Chow, 1990):

Table 1. State variables and associated thermodynamic forces

State variables	Associated thermodynamic forces
Elastic strain $\underline{\varepsilon}_e$	Cauchy stress $\underline{\sigma}$
Accumulated plastic strain α	Plastic hardening threshold R
Damage variable $\underline{D} = (D_1, D_2, D_3)$	Damage energy release rate $\underline{Y} = (Y_1, Y_2, Y_3)$
Overall damage β	Damage strengthening threshold B
Temperature T	Entropy S

$$\rho\psi(\underline{\sigma}, \underline{D}, \alpha, \beta) = W_e(\underline{\sigma}_e, \underline{D}) + \psi_p(\alpha) + \psi_d(\beta) \tag{8}$$

where $W_e(\underline{\varepsilon}_e, \underline{D})$ is the elastic strain energy, $\psi_p(\alpha)$ the free energy due to plastic hardening and $\psi_d(\beta)$ the free energy due to damage hardening. The complementary energy is obtained from the Legendre transformation of the free energy with respect to strain, i.e.

$$\rho\Pi(\underline{\sigma}, \underline{D}, \alpha, \beta) = \underline{\sigma} : \underline{\varepsilon}_e - \rho\psi(\underline{\varepsilon}_e, \underline{D}, \alpha, \beta) = W_e(\underline{\sigma}, \underline{D}) - \psi_p(\alpha) - \psi_d(\beta). \tag{9}$$

According to the energy equivalence hypothesis, the elastic strain energy $W_e(\underline{\varepsilon}_e, \underline{D})$ and the complementary elastic energy $W_e(\underline{\sigma}, \underline{D})$ can be evaluated as:

$$W_e(\underline{\varepsilon}_e, \underline{D}) = W_e(\bar{\underline{\varepsilon}}) = \tfrac{1}{2}\bar{\underline{\varepsilon}}_e^T \underline{C}_e \bar{\underline{\varepsilon}}_e = \tfrac{1}{2}\underline{\varepsilon}_e^T \underline{M}^{-1} \underline{C}_e \underline{M}^{-1} \underline{\varepsilon}_e \tag{10a}$$

$$W_e(\underline{\sigma}, \underline{D}) = W_e(\bar{\underline{\sigma}}) = \tfrac{1}{2}\bar{\underline{\sigma}}^T \underline{C}_e^{-1} \bar{\underline{\sigma}} = \tfrac{1}{2}\underline{\sigma}^T \underline{M} \underline{C}_e^{-1} \underline{M} \underline{\sigma}. \tag{10b}$$

Following the rules of thermodynamics of irreversible processes, the associated thermodynamic forces are given by:

$$\underline{\sigma} = \frac{\rho\partial\psi}{\partial\underline{\varepsilon}_e} = \underline{M}^{-1} \underline{C}_e \underline{M}^{-1} \underline{\varepsilon}_e$$

$$R = \rho\frac{\partial\psi}{\partial\alpha} = \frac{\partial\psi_p(\alpha)}{\partial\alpha}$$

$$B = \rho\frac{\partial\psi}{\partial\beta} = \frac{\partial\psi_d(\beta)}{\partial\beta}$$

$$\underline{Y} = \rho\frac{\partial\psi}{\partial\underline{D}} = -\rho\frac{\partial\Pi}{\partial\underline{D}} = -\frac{\partial W_e(\underline{\sigma}, \underline{D})}{\partial\underline{D}} = -\underline{\sigma}^{\mathrm{T}} \underline{M} \underline{C}_{\mathrm{e}}^{-1} \frac{\partial\underline{M}}{\partial\underline{D}} \underline{\sigma}. \tag{11}$$

The negative of $\underline{Y}$ can be considered as the elastic strain energy rate associated with a unit damage increment as it is easy to show that:

$$-\underline{Y} = \frac{1}{2}\frac{\mathrm{d}W_e}{(\mathrm{d}\underline{D})}\Bigg]_{\text{at constant } \underline{\sigma}}. \tag{12}$$

$\underline{Y}$ is often given the name of "damage energy release rate" in view of the energy relation in eqn (12) (Lemaitre and Chaboche, 1985).

3.3. *The dissipation power*

According to the second law of thermodynamics, the total dissipation power with convexity and normality properties is:

$$\Phi = \underline{\sigma}\,\dot{\underline{\varepsilon}}_p - R\dot{\alpha} - \underline{Y}\dot{\underline{D}} - B\dot{\beta} \geqslant 0. \tag{13}$$

Within the hypotheses of uncoupling between mechanical and thermal dissipations and of independence of energy dissipations between plastic flow and damage processes, eqn (13) can be separated into two parts such that:

$$\underline{\sigma}\,\dot{\underline{\varepsilon}}_p - R\dot{\alpha} \geqslant 0 \tag{14a}$$

$$-\underline{Y}\dot{\underline{D}} - B\dot{\beta} \geqslant 0. \tag{14b}$$

Equations (14a) and (14b) show that there exists a plastic dissipative potential and a damage dissipative potential, i.e.

$$F_p(\underline{\sigma}, \underline{D}, R) = 0 \tag{15}$$

$$F_d(\underline{Y}, \underline{B}) = 0 \tag{16}$$

in which the former represents the plastic yield criterion; the latter is the damage evolution criterion. In case the criteria $F_p = 0$ and $F_d = 0$ are satisfied, the actual values of $\underline{\sigma}$, R, $\underline{Y}$, B will make the dissipation power of eqn (13) a stationary value.

If we introduce Lagrange multipliers $\dot{\lambda}_p$ and $\dot{\lambda}_d$ eqn (13) can be written:

$$\Phi = \underline{\sigma}\,\underline{\dot{\varepsilon}}_p - R\dot{\alpha} - \underline{Y}\,\underline{\dot{D}} - B\dot{\beta} - \dot{\lambda}_p F_p - \dot{\lambda}_d F_d. \tag{17}$$

Thus we have:

$$\begin{aligned}
&\frac{\partial \Phi}{\partial \underline{\sigma}} = 0 \Rightarrow \underline{\dot{\varepsilon}}_p = \dot{\lambda}_p \frac{\partial F_p}{\partial \underline{\sigma}} \\
&\frac{\partial \Phi}{\partial R} = 0 \Rightarrow \dot{\alpha} = -\dot{\lambda}_p \frac{\partial F_p}{\partial R} \\
&\frac{\partial \Phi}{\partial \underline{Y}} = 0 \Rightarrow \underline{\dot{D}} = -\dot{\lambda}_d \frac{\partial F_d}{\partial \underline{Y}} \\
&\frac{\partial \Phi}{\partial B} = 0 \Rightarrow \dot{\beta} = -\dot{\lambda}_d \frac{\partial F_d}{\partial B}.
\end{aligned} \tag{18}$$

4. FULLY COUPLED ANISOTROPIC ELASTO-VISCO-PLASTIC DAMAGE MODEL

4.1. *Anisotropic elasticity and damage*

When a material is damaged, the constitutive relation is:

$$\underline{\sigma} = \underline{\bar{C}}_e \underline{\varepsilon}_e. \tag{19}$$

Comparison between eqns (11a) and (19), gives:

$$\underline{\bar{C}}_e = \underline{M}^{-1}\,\underline{C}_e\,\underline{M}^{-1}. \tag{20}$$

Since the elastic tensor $\underline{C}_e$ is symmetric, $\underline{\bar{C}}_e$ is symmetric too. The elastic tensor $\underline{C}_e$ may be represented by a 6×6 matrix. For orthotropic materials:

$$\underline{C}_e^{-1} = \begin{bmatrix}
\frac{1}{E_1} & -\frac{\nu_{21}}{E_2} & -\frac{\nu_{31}}{E_3} & 0 & 0 & 0 \\
-\frac{\nu_{12}}{E_1} & \frac{1}{E_2} & -\frac{\nu_{32}}{E_3} & 0 & 0 & 0 \\
-\frac{\nu_{13}}{E_1} & -\frac{\nu_{23}}{E_2} & \frac{1}{E_3} & 0 & 0 & 0 \\
0 & 0 & 0 & \frac{1}{G_{23}} & 0 & 0 \\
0 & 0 & 0 & 0 & \frac{1}{G_{31}} & 0 \\
0 & 0 & 0 & 0 & 0 & \frac{1}{G_{12}}
\end{bmatrix} \tag{21}$$

with

$$\frac{\nu_{12}}{E_1}=\frac{\nu_{21}}{E_2},\quad \frac{\nu_{31}}{E_3}=\frac{\nu_{13}}{E_1},\quad \frac{\nu_{32}}{E_3}=\frac{\nu_{23}}{E_2}. \tag{22}$$

Thus, $\underline{C}_e$ is:

$$\underline{C}_e=\begin{bmatrix} \frac{E_1(1-\nu_{32}\nu_{23})}{\Delta_c} & \frac{E_2(\nu_{12}+\nu_{13}\nu_{32})}{\Delta_c} & \frac{E_3(\nu_{13}+\nu_{12}\nu_{23})}{\Delta_c} & 0 & 0 & 0 \\ \frac{E_1(\nu_{21}+\nu_{23}\nu_{31})}{\Delta_c} & \frac{E_2(1-\nu_{13}\nu_{31})}{\Delta_c} & \frac{E_3(\nu_{23}+\nu_{21}\nu_{13})}{\Delta_c} & 0 & 0 & 0 \\ \frac{E_1(\nu_{31}+\nu_{21}\nu_{32})}{\Delta_c} & \frac{E_2(\nu_{32}+\nu_{12}\nu_{31})}{\Delta_c} & \frac{E_3(1-\nu_{21}\nu_{12})}{\Delta_c} & 0 & 0 & 0 \\ 0 & 0 & 0 & G_{23} & 0 & 0 \\ 0 & 0 & 0 & 0 & G_{31} & 0 \\ 0 & 0 & 0 & 0 & 0 & G_{12} \end{bmatrix} \tag{23}$$

where:

$$\Delta_c=1-\nu_{21}\nu_{12}-\nu_{31}\nu_{13}-\nu_{32}\nu_{23}-\nu_{12}\nu_{23}\nu_{31}-\nu_{21}\nu_{13}\nu_{32}.$$

Because of symmetric properties, we have the following relations from eqn (22):

$$E_1(\nu_{21}+\nu_{23}\nu_{31})=E_2(\nu_{12}+\nu_{13}\nu_{32}),\ E_1(\nu_{31}+\nu_{21}\nu_{32})=E_3(\nu_{13}+\nu_{12}\nu_{23})$$
$$E_2(\nu_{32}+\nu_{12}\nu_{31})=E_3(\nu_{23}+\nu_{21}\nu_{13}). \tag{24}$$

In order to guarantee the positive definiteness of $\bar{\underline{C}}_e$, the following conditions should be satisfied

$$0<\Delta_c\leqslant 1,\quad 0<1-\nu_{ij}\nu_{ji}\leqslant 1\quad (\text{no sum on } i,j),\quad 0\leqslant D_i<1$$
$$G_{23}>0,\quad G_{31}>0,\quad G_{12}>0,\quad E_1>0,\quad E_2>0,\quad E_3>0. \tag{25}$$

4.2. *Anisotropic plastic yield surface*

In the damage characterization of materials undergoing large plastic deformations, Hill's yield criterion in stress space is expressed in the following form:

$$F_p(\underline{\sigma},\underline{D},R)=F_p(\bar{\underline{\sigma}},R)=\bar{\sigma}_F-R_0-R(\alpha)=0 \tag{26}$$

where R_0 is the initial strain hardening threshold.

The effective equivalent stress $\bar{\sigma}_F$ is:

$$\bar{\sigma}_F=\{\tfrac{1}{2}\bar{\underline{\sigma}}^T\underline{\underline{H}}\,\bar{\underline{\sigma}}\}^{1/2}=\{\tfrac{1}{2}\underline{\sigma}^T\underline{\underline{\bar{H}}}\,\underline{\sigma}\}^{1/2}. \tag{27}$$

The effective plastic characteristic tensor $\underline{\underline{\bar{H}}}$ is given by:

$$\underline{\underline{\bar{H}}}=\underline{\underline{M}}(\underline{D})\,\underline{\underline{H}}\,\underline{\underline{M}}(\underline{D}). \tag{28}$$

The positive definite tensor $\underline{\underline{H}}$ for orthotropic materials is represented by a 6×6 matrix as in the material principal coordinate system (Hill, 1950).

$$\underline{H} = \begin{bmatrix} G+H & -H & -G & 0 & 0 & 0 \\ -H & H+F & -F & 0 & 0 & 0 \\ -G & -F & F+G & 0 & 0 & 0 \\ 0 & 0 & 0 & N & 0 & 0 \\ 0 & 0 & 0 & 0 & L & 0 \\ 0 & 0 & 0 & 0 & 0 & M \end{bmatrix} \tag{29}$$

where F, G, H, L, M, N are parameters characterizing the current state of plastic anisotropy. For a strain-hardening material, the uniaxial yield stress varies with increasing plastic deformation, and therefore the anisotropic parameters should also vary, since they are functions of the current yield stress (see Valliappan *et al.*, 1976). The consistency between the general thermodynamic framework and treatment of anisotropic hardening require tensor $\underline{H}$ being a state variable. However, this will make the solution very complicated. Since we work with weak degree of anisotropy, $\underline{H}$ in plastic flow rule eqn (30) could be treated as constant tensor.

The plastic constitutive equations incorporating material damage may be derived by taking the yield criterion [eqn (26)] as a potential function. By assuming an associated flow rule, the rate-independent damage plastic response is characterized as follows:

$$\left\{ \dot{\underline{\varepsilon}}_p = \dot{\lambda}_p \frac{\partial F_p}{\partial \underline{\sigma}} = \frac{\underline{M}\,\underline{H}\,\underline{M}\,\underline{\sigma}}{2\bar{\sigma}_F} \dot{\lambda}_p \right. \quad \text{(plastic flow rule)} \tag{30}$$

$$\left\{ \dot{R} = \dot{\lambda}_p \frac{\mathrm{d}R}{\mathrm{d}\alpha} \right. \quad \text{(isotropic hardening rule)} \tag{31}$$

$$\left\{ F_p \leqslant 0, \dot{\lambda}_p \geqslant 0, \dot{\lambda}_p F_p = 0 \right. \quad \text{(plastic loading/unloading rule)} \tag{32}$$

4.3. *Damage evolution law and damage surface*

4.3.1. *Damage evolution surface.* In a similar way to the arguments leading to plastic dissipative potential, one can assume that there exists a surface $F_d = 0$, which separates the damaging domain from the undamaging domain. A damage criterion in a quadratic homogeneous function of the damage energy release rate $\underline{Y}$ was proposed as (Cordebois and Sidoroff, 1979, 1982 and 1983):

$$F_d = Y_{eq} - B_0 - B(\beta) = 0 \tag{33}$$

where the equivalent damage energy release rate Y_{eq} is defined by:

$$Y_{eq} = [\tfrac{1}{2} \underline{Y}^{\mathrm{T}} \underline{J}\, \underline{Y}]^{1/2} \tag{34}$$

in which $\underline{J}$ is the damage characteristic tensor.

4.3.2. *Damage characteristic tensor* $\underline{J}$. One remaining parameter yet to be defined in eqn (34) is the damage characteristic tensor $\underline{J}$. Normally, $\underline{J}$ seems to be a fourth order tensor [as $\underline{H}$ in eqn (27)]. However, since we work on the principal coordinate system of damage as $Y_{12} = Y_{23} = Y_{31} = 0$, it can be treated like a second order tensor. Furthermore, this tensor can be assumed to be symmetric; the operator in its general form has six

independent components. Such a tensor will render the formulation of the constitutive equations too complicated for general engineering applications for which simplifications become necessary.

The determination of a suitable damage characteristic tensor $\underline{J}$, which is simple enough to be applied and yet describes accurately the nonlinear nature of damage growth, may well be the most important aspect in the present formulation of anisotropic damage evolution law.

The purpose of introducing a damage characteristic tensor $\underline{J}$, like the introduction of plastic characteristic tensor $\underline{H}$ in the theory of plasticity, is to take account of the anisotropic nature of damage growth.

(1) In order to retain eqn (34), it must be a positive semi-definite tensor.

(2) In order to satisfy the thermodynamic condition $\underline{\dot{D}} \geqslant 0$ [see eqn (45)] each term D_i ($i = 1,2,3$) must positive for all loading spectrums, hence

$$J_{ij} \geqslant 0. \tag{35}$$

(3) Next, it must reduce to a scalar equation when the damage response is isotropic and represented by $D_1 = D_2 = D_3$.

(4) Furthermore, the components of $\underline{J}$ are generally not material constants (Lu and Chow 1990).

Since the several existing formulations of $\underline{J}$ are of a more or less simplified nature, a new form of $\underline{J}$ which satisfies the above requirements will be proposed and its physical implications clarified. The damage characteristic tensor $\underline{J}$ in the Cordebois–Sidoroff model was expressed as:

$$\underline{J} = \begin{bmatrix} 1 & 0 & 0 \\ 0 & \mu & 0 \\ 0 & 0 & \mu \end{bmatrix}, \quad 0 \leqslant \mu \leqslant 1 \tag{36}$$

where μ is a material constant. It reduces to a scalar equation, only if $\mu = 1$.

Lee *et al.* (1985) proposed to use the following form of $\underline{J}$:

$$\underline{J} = \begin{bmatrix} 1 & \mu & \mu \\ \mu & 1 & \mu \\ \mu & \mu & 1 \end{bmatrix} \tag{37}$$

to describe anisotropic damage evolution. However, their assumption that μ is a material constant is not realistic (Lu and Chow, 1990).

Recently, Chow and Lu (1989a) proposed the following generalized expression for $\underline{J}$:

$$\underline{J} = 2\begin{bmatrix} 1 & J_{12} & J_{12} \\ J_{12} & 1 & J_{12} \\ J_{12} & J_{12} & 1 \end{bmatrix} \tag{38}$$

which has only one unknown parameter to be determined from a standard tensile test:

$$J_{12} = \frac{\mathrm{d}D_1}{\mathrm{d}D_2}\bigg]_{\mathrm{d}\sigma_2 = 0} = \frac{\mathrm{d}D_2}{\mathrm{d}D_1}\bigg]_{\mathrm{d}\sigma_1 = 0}. \tag{39}$$

However, it is only suited for the case when the virgin material properties are isotropic. A new damage characteristic tensor $\underline{J}$, similar to the plastic characteristic tensor $\underline{H}$ in the theory of plasticity, with more general properties and more rational physical significance

than the previous formulation due to (Cordebois, 1983; Lee *et al.*, 1985; Chow and Lu, 1989a) is proposed on the basis of the damage energy equivalence:

$$\underline{J} = 2\begin{bmatrix} 1 & \sqrt{J_2} & \sqrt{J_3} \\ \sqrt{J_2} & J_2 & \sqrt{J_2 J_3} \\ \sqrt{J_3} & \sqrt{J_2 J_3} & J_3 \end{bmatrix}. \tag{40}$$

In the case of damage hardening materials, the equivalent damage energy release rate increases with increasing total damage growth, and hence, the anisotropic parameters in eqn (40) should also vary. The change in the equivalent energy release rate in any component depends on the total amount of damage work done in that component. For an equivalent variation, the damage work done in each component should be the same. For the case of a linear damage hardening as shown in Fig. 1, the damage work in component 1 is:

$$W_{d1} = \frac{1}{2} D_1 (Y_{10} + Y_1) = \frac{1}{2} \frac{(Y_1 - Y_{10})}{D_{t1}} (Y_{10} + Y_1) = \frac{1}{2D_{t1}} (Y_1^2 - Y_{10}^2). \tag{41}$$

Similarly the damage work done in terms of equivalent damage energy release rate Y_{eq} is:

$$W_d = \frac{1}{2D_t} (Y_{eq}^2 - Y_0^2). \tag{42}$$

By equating eqns (41) and (42), we have:

$$a_1 = \left(\frac{Y_{eq}}{Y_1}\right)^2 = \frac{Y_{eq}^2}{(D_{t1}/D_t)(Y_{eq}^2 - Y_0^2) + Y_{10}^2}. \tag{43a}$$

Similarly:

$$a_2 = \left[\frac{Y_{eq}}{Y_2}\right]^2 = \frac{Y_{eq}^2}{(D_{t2}/D_t)(Y_{eq}^2 - Y_0^2) + Y_{20}^2} \tag{43b}$$

$$a_3 = \left[\frac{Y_{eq}}{Y_3}\right]^2 = \frac{Y_{eq}^2}{(D_{t3}/D_t)(Y_{eq}^2 - Y_0^2) + Y_{30}^2}. \tag{43c}$$

Obviously, if component 1 coincides with the reference component, $B_0 = Y_{10}$, $B(\beta) = Y_1 - Y_{10}$, $a_1 = 1$ and

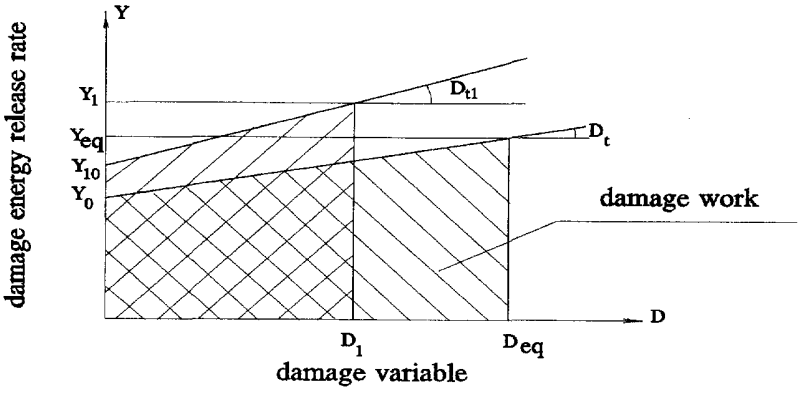

Fig. 1. Equating damage work.

$$J_2 = a_2 = \frac{Y_1^2}{(D_{t2}/D_{t1})(Y_1^2 - Y_{10}^2) + Y_{20}^2}$$
$$J_3 = a_3 = \frac{Y_1^2}{(D_{t3}/D_{t1})(Y_1^2 - Y_{10}^2) + Y_{30}^2}. \tag{44}$$

In the above equations, D_{ti} are the slopes of Y_i–D_i curves with component i; Y_i the current equivalent damage energy release rate corresponding to component i; Y_{i0} the initial equivalent damage energy release rate corresponding to component i.

Obviously, the damage characteristic tensor $\underline{J}$ in eqn (40) with the parameters in eqn (44) satisfy the four requirements mentioned above. $\underline{J}$ may be handled as a constant tensor in the damage evolution rule [eqn (45)], similar to the discussion in Section 4.2. for tensor $\underline{H}$, in order to avoid complex derivation. This treatment may violate the thermodynamic consistency. However, comparisons between simulation and experiment show that this treatment gives interesting results.

4.3.3. *Evolution law of anisotropic damage.* In much the same way as the definition of plastic flow, the evolution law of anisotropic damage is characterized below:

$$\begin{cases} \underline{\dot{D}} = -\dot{\lambda}_d \dfrac{\partial F_d}{\partial \underline{Y}} = -\dfrac{\underline{J}\,\underline{Y}}{2Y_{eq}}\dot{\lambda}_d = \underline{Y}^*\dot{\lambda}_d \\ \text{with } Y^* = -\dfrac{\underline{J}\,\underline{Y}}{2Y_{eq}} \\ \text{(damage evolution rule)} \end{cases} \tag{45}$$

$$\begin{cases} \dot{\beta} = -\dot{\lambda}_d \dfrac{\partial F_d}{\partial B} = \dot{\lambda}_d \\ \dot{B} = \dfrac{\mathrm{d}B}{\mathrm{d}\beta}\dot{\beta} = \dfrac{\mathrm{d}B}{\mathrm{d}\beta}\dot{\lambda}_d \\ \text{(damage hardening rule)} \end{cases} \tag{46}$$

$$\begin{cases} F_d \leqslant 0, \\ \dot{\lambda}_d \geqslant 0, \\ \dot{\lambda}_d F_d = 0. \end{cases} \tag{47}$$

(damage loading/unloading rule)

4.4. *Constitutive relations for elastoplastic damage*

According to the elastic constitutive relations [eqn (19)] and to the effective stress tensor definition [eqn (1)], we have:

$$\underline{\bar{\sigma}} = \underline{C}_e\,\underline{M}^{-1}\,\underline{\varepsilon}_e. \tag{48}$$

Noting the relations:

$$\underline{\dot{\varepsilon}} = \underline{\dot{\varepsilon}}_e + \underline{\dot{\varepsilon}}_p \tag{49}$$

and:

$$\underline{\dot{M}}^{-1} = -\underline{M}^{-1}\,\underline{\dot{M}}\,\underline{M}^{-1} \tag{50}$$

with eqns (48, 49, 50, 19) the objective rate form of eqn (48) is:

$$\overset{\nabla}{\underline{\sigma}} = \underline{C}_e \underline{M}^{-1} \dot{\underline{\varepsilon}}_e + \underline{C}_e \dot{\underline{M}}^{-1} \underline{\varepsilon}_e = \underline{C}_e \underline{M}^{-1} \dot{\underline{\varepsilon}} - \underline{C}_e \underline{M}^{-1} \dot{\underline{\varepsilon}}_p - \underline{C}_e \underline{M}^{-1} \dot{\underline{M}} \underline{C}_e^{-1} \underline{M} \underline{\sigma}. \tag{51}$$

According to eqn (45), we have:

$$\dot{\underline{M}} = \frac{\partial \underline{M}}{\partial \underline{D}} \dot{\underline{D}} = -\left[\frac{\partial \underline{M}}{\partial \underline{D}} \frac{\underline{J}\,\underline{Y}}{2Y_{eq}}\right] \dot{\lambda}_d = \underline{A}^* \dot{\lambda}_d \tag{52}$$

with:

$$\underline{A}^* = -\frac{\partial \underline{M}}{\partial \underline{D}} \frac{\underline{J}\,\underline{Y}}{2Y_{eq}}. \tag{53}$$

Substituting eqns (30) and (52) into eqn (51), we obtain:

$$\overset{\nabla}{\underline{\sigma}} = \underline{C}_e \underline{M}^{-1} \dot{\underline{\varepsilon}} - \underline{C}^* \dot{\lambda}_p - \underline{D}^* \dot{\lambda}_d \tag{54}$$

where:

$$\underline{C}^* = \frac{\underline{C}_e \underline{H} \underline{M} \underline{\sigma}}{2\bar{\sigma}_F} \tag{55}$$

$$\underline{D}^* = \underline{C}_e \underline{M}^{-1} \underline{A}^* \underline{C}_e^{-1} \underline{M} \underline{\sigma} \tag{56}$$

thus:

$$\overset{\nabla}{\underline{\sigma}} = \underline{M}^{-1} \overset{\nabla}{\underline{\sigma}} - \underline{M}^{-1} \dot{\underline{M}} \underline{\sigma} = \underline{M}^{-1} \underline{C}_e \underline{M}^{-1} \dot{\underline{\varepsilon}} - \underline{E}^* \dot{\lambda}_p - \underline{F}^* \dot{\lambda}_d \tag{57}$$

in which:

$$\underline{E}^* = \underline{M}^{-1} \underline{C}^* = \frac{\underline{M}^{-1} \underline{C}_e \underline{H} \underline{M} \underline{\sigma}}{2\bar{\sigma}_F} \tag{58}$$

$$\underline{F}^* = \underline{M}^{-1} \underline{D}^* + \underline{M}^{-1} \underline{A}^* \underline{\sigma}. \tag{59}$$

According to eqn (11d), we can write:

$$-\underline{Y} = \underline{\sigma}^T \underline{Z}^* \underline{\sigma} \tag{60}$$

where:

$$\underline{Z}^* = \underline{M} \underline{C}_e^{-1} \frac{\partial \underline{M}}{\partial \underline{D}}. \tag{61}$$

The rate of eqn (60) is:

$$-\underline{\dot{Y}} = 2\underline{\sigma}^T \underline{Z}^* \overset{\nabla}{\underline{\sigma}} + \underline{\sigma}^T \left(\frac{\partial \underline{Z}^*}{\partial \underline{D}} \underline{\dot{D}} \right) \underline{\sigma} = \underline{J}^* \underline{\dot{\varepsilon}} + \underline{H}^* \dot{\lambda}_p + \underline{T}^* \dot{\lambda}_d \tag{62}$$

where [with eqn (45)]:

$$\underline{J}^* = 2\underline{\sigma}^T \underline{Z}^* \underline{M}^{-1} \underline{C}_e \underline{M}^{-1} \tag{63}$$

$$\underline{H}^* = -2\underline{\sigma}^T \underline{Z}^* \underline{E}^* \tag{64}$$

$$\underline{T}^* = -2\underline{\sigma}^T \underline{Z}^* \underline{F}^* + \underline{\sigma}^T \left(\frac{\partial \underline{Z}^*}{\partial \underline{D}} \underline{Y}^* \right) \underline{\sigma}. \tag{65}$$

Now, the fully coupled elastoplastic damage constitutive equations are summarized as below:

$$\underline{\dot{\varepsilon}} = \underline{\dot{\varepsilon}}_e + \underline{\dot{\varepsilon}}_p$$

$$\overset{\nabla}{\underline{\sigma}} = \underline{M}^{-1} \underline{C}_e \underline{M}^{-1} \underline{\dot{\varepsilon}} - \underline{E}^* \dot{\lambda}_p - \underline{F}^* \dot{\lambda}_d$$

$$\underline{\dot{\varepsilon}}_p = \frac{\underline{M}\,\underline{H}\,\underline{M}\,\underline{\sigma}}{2\bar{\sigma}_F} \dot{\lambda}_p$$

$$\dot{\alpha} = \dot{\lambda}_p$$

$$\dot{R} = \dot{\lambda}_p \frac{\mathrm{d}R}{\mathrm{d}\alpha}$$

$$-\underline{\dot{Y}} = \underline{J}^* \underline{\dot{\varepsilon}} + \underline{H}^* \dot{\lambda}_p + \underline{T}^* \dot{\lambda}_d$$

$$\underline{\dot{D}} = -\frac{\underline{J}\,\underline{Y}}{2\,Y_{eq}} \dot{\lambda}_d$$

$$\dot{\beta} = \dot{\lambda}_d$$

$$\dot{B} = \frac{\mathrm{d}B}{\mathrm{d}\beta} \dot{\lambda}_d$$

$$F_p = \left\{ \frac{1}{2} \underline{\sigma}^T \underline{M}\,\underline{H}\,\underline{M}\,\underline{\sigma} \right\}^{\frac{1}{2}} - R_0 - R(\alpha) = \left\{ \frac{1}{2} \underline{\bar{\sigma}}^T \underline{H}\,\underline{\bar{\sigma}} \right\}^{\frac{1}{2}} - R_0 - R(\alpha) = 0$$

$$F_d = \left\{ \frac{1}{2} \underline{Y}^T \underline{J}\,\underline{Y} \right\}^{\frac{1}{2}} - B_0 - B(\beta) = 0. \tag{66}$$

4.5. *Anisotropic microcrack opening and closing mechanisms*

It is generally admitted that only tensile strains in the strain principal directions contribute to microcrack growth, especially for various brittle materials. Simo and Ju (1987a,b) and Ju (1989a,b) proposed an approach of spectral decomposition of the strain tensor for their strain-based damage model (Simo and Ju, 1987a,b) and energy-based damage model (Ju, 1989a,b), to consider different mechanisms under tensile and compressive states.

The treatment here is similar to the previous proposal of Simo and Ju, but with the spectral decomposition of the stress tensor for our present energy-based damage model.

First, in view of the significance of tensile strains in damage processes, we propose the following definition for the tensile stress tensor $\underline{\sigma}^+$. Consider the spectral decomposition of the stress tensor:

$$\underline{\sigma} = \sum_{i=1}^{3} \sigma_i \underline{P}_i \otimes \underline{P}_i, \quad |\underline{P}_i| = 1 \tag{67}$$

where σ_i is the i-th principal stress and $\underline{P}_i$ the i-th corresponding unit principal direction. Let $\underline{Q}$ and $\underline{Q}^+$, separately, be the regular and positive (tensile) spectral projection tensors defined as:

$$\underline{Q} = \sum_{i=1}^{3} \underline{P}_i \otimes \underline{P}_i; \quad \underline{Q}^+ = \sum_{i=1}^{3} \hat{H}(\sigma_i)\, \underline{P}_i \otimes \underline{P}_i \tag{68}$$

where $\hat{H}(.)$ is the Heaviside step function. In addition, the fourth-order positive projection tensor $\underline{P}^+$ is defined with components (see also Simo and Ju, 1987a),

$$P^+_{ijkl} = Q^+_{ia}\, Q^+_{jb}\, Q_{ka}\, Q_{lb} \tag{69}$$

so that the so-called tensile tensor $\underline{\sigma}^+$ can be expressed as:

$$\underline{\sigma}^+ = \underline{P}^+ \underline{\sigma}, \quad \text{i.e.} \quad \sigma^+_{ij} = P^+_{ijkl}\, \sigma_{kl}. \tag{70}$$

With this notation at hand, the damage energy release rate $\underline{Y}$ in eqn (60) can also be modified as follows to accommodate "ductile" like and "brittle" like material damage.

$$-\underline{Y} = \begin{cases} \underline{\sigma}^T \underline{Z}^* \underline{\sigma} & \text{(ductile-like damage)} \\ \underline{\sigma}^{+T} \underline{Z}^* \underline{\sigma}^+ & \text{(brittle-like damage)} \end{cases}. \tag{71}$$

Here, roughly speaking, "ductile-like damage" material means that in such materials, the effects of compressive and tensile states are the same to damage growth; "brittle-like damage" material means that only the tensile components contribute to the evolution of damage in such materials. It should emphasized that the words "ductile-like damage" and "brittle-like damage" are merely definitions for two types of damage growth and do not imply an assumption on the ductility (capacity to have large strains before rupture) or the brittleness of the material itself.

Furthermore, eqn (62) may be expressed in the form:

$$-\dot{\underline{Y}} = \begin{cases} 2\underline{\sigma}^T \underline{Z}^* \overset{\nabla}{\underline{\sigma}} + \underline{\sigma}^T \left(\dfrac{\partial \underline{Z}^*}{\partial \underline{D}} \underline{\dot{D}} \right)^s \underline{\sigma} & \text{(ductile-like damage)} \\ 2\underline{\sigma}^{+T} \underline{Z}^* \overset{\nabla}{\underline{\sigma}}^+ + \underline{\sigma}^{+T} \left(\dfrac{\partial \underline{Z}^*}{\partial \underline{D}} \underline{\dot{D}} \right)^s \underline{\sigma}^+ & \text{(brittle-like damage)} \end{cases}. \tag{72}$$

Obviously, for brittle-like damage, if all three principal strains σ_i are tensile, then the local microcracks are active in all three principal directions. On the other hand, if all σ_i are compressive, no growth of microcracks occurs under the current state. Clearly, other combinations of tensile and compressive states will give rise to various microcrack "opening" and "closing" situations.

The above discussion on microcrack closure, eqns (67) to (70), is somehow similar to the proposal of Ortiz (1985). There exist nevertheless two significant differences between the two formulations:

(1) Ortiz's model only treats brittle materials.

(2) Ortiz's formulation focused on the rate of a so-called "added compliance tensor" while the present proposal focuses on the damage evolution laws. It is emphasized that the two procedures are not equivalent.

(3) The explicit form of the positive orthogonal projection tensor $\underline{P}^+$ in eqn (69) is a nonlinear, non-constant operator associated with the current total stress tensor $\underline{\sigma}$ which is more precise than that given in Ortiz's model (Ju, 1989a).

4.6. *Extension to fully coupled elasto-visco-plastic damage model*

4.6.1. *Objective and background of this study.* Material response behaviour under high strain rates is needed for a range of current applications. Aircraft and vehicles are generally subjected to impact loading which often brings failures and serious damages in their components. It is well-known that strain rate, strain rate history and temperature effects play an important part in stress–strain relations under high speed loading. Some existing experimental results also show that the amount of microcracking (damage) at a particular strain level exhibits rate sensitivity to the applied rate of loading in a (high strain rate) dynamic environment (Simo and Ju, 1987a). On the other hand, it has long been recognized that rate-independent constitutive laws are inadequate in the modelling of hot-forming processes.

Hence, the necessity of using appropriate rate-dependent constitutive models, which include the rate and rate-history effects, is obvious.

There are many viscoplastic models in the recent literature for dynamic material behaviour at high strain rate. The important features of dynamic material behaviour such as strain rate, strain rate history and temperature dependence were described with emphasis on a comparison of theoretical and experiments results in a recent bibliographic research (Zhu and Cescotto, 1992).

One of the simplest unified viscoplastic models was proposed by Perzyna (1971), under multiaxial conditions. However, Perzyna's approach is generally not well suited for non-smooth multi-surface rate-dependent plasticity models (Simo *et al.*, 1988; Ju, 1990a). This is due to the fact that, in the "corner regions" of non-smooth multi-surface plasticity models, the family of nested viscoplastic loading surfaces (outside the static yield surface) are neither clearly nor uniquely defined. Thus, the loading/unloading conditions may not be appropriate for the Perzyna-type multi-surface viscoplasticity models (Simo *et al.*, 1988). In fact, as the viscosity parameter approaches zero, the Perzyna-type model would not reduce to the rate independent plasticity formulation in the case of non-smooth multi-surface modes.

To remedy this shortcoming, an alternative (non-equivalent) viscoplasticity formulation was proposed by Duvaut and Lions (1972), and was recently further enhanced by Simo *et al.* (1988) and Ju (1990a). It is noted that the Duvaut–Lions viscoplasticity model does not utilize the concept of nested viscoplastic loading surfaces and thus precludes the difficulty encountered by the Perzyna-type models in non-smooth corner regions.

There exists one plastic yield surface and a damage evolution surface in the present elastoplastic damage model. Thus, non-smooth corner regions at the intersection of these surfaces can be observed. Due to the same non-smooth corner phenomenon as in non-smooth multisurface plasticity models, we will use the viscoplastic regularization of the Duvaut–Lions type proposed by Ju and Simo *et al.* for the structure of the viscous regularization of the previously developed rate-independent elastoplastic damage model. The resulting rate-sensitive elastoplastic damage model requires one additional material parameter, i.e. the viscosity coefficient μ. As μ approaches zero it reduces to the rate independent elastoplastic damage model, whereas as μ approaches infinity it exhibits instantaneous elastic response.

Of course, with such a simple approach, complex viscous material behaviours cannot be modelled with high precision. It must therefore be considered as a first and approximative representation of the strain rate effects.

Another reason to use the viscous regularization in our rate-independent damage model is to preserve the uniqueness of finite element solution (Benallal *et al.*, 1991). It is now well-known that there are unique well-posed numerical convergence problems in computations associated with apparently "strain softening" material due to the loss of ellipticity at the level of material constitutive equations. In fact, in viscous models, there are no plastic and damage consistency conditions, thus no strain rate jumping phenomenon (Benallal *et al.*, 1991) and the numerical difficulties may be avoided (Loret and Prevost, 1990; Prevost and Loret, 1990).

4.6.2. *Extension of the Duvaut–Lions model by Simo.* The rate constitutive equations of the Duvaut–Lions type viscoplasticity postulated by Simo *et al.* (1988) are:

$$\underline{\dot{\varepsilon}}_{vp} = \frac{1}{\mu}\underline{C}_e^{-1} : (\underline{\sigma} - \underline{\sigma}^*), \quad \dot{q} = -\frac{1}{\mu}(\underline{q} - \underline{q}^*) \quad \text{if} \quad F_p(\underline{\sigma}, \underline{q}) > 0 \tag{73}$$

where $\underline{\dot{\varepsilon}}_{vp}$ is the viscoplastic strain rate tensor, μ the viscosity coefficient, $\underline{C}_e$ the elasticity tensor, $\underline{\sigma}$ the current stress tensor, $\underline{q}$ a set of plastic variables, $(\underline{\sigma}^*, \underline{q}^*)$ the non-viscid solution of the rate-independent elastoplastic problem, and F_p the static yield surface. With proper loading/unloading conditions, the generalized Duvaut–Lions model renders a definite and unique viscoplastic solution even in the corner regions. Clearly, the viscoplastic solution should lie between "the elastic predictor" and the "non-viscid plastic solution".

Two unconditionally stable constitutive integration algorithms for the generalized Duvaut–Lions viscoplasticity model were proposed by Simo *et al.* (1988), including the implicit backward Euler and the "full integration" algorithms. For the sake of clarity and simplicity, only the implicit backward Euler algorithm is used in our present model although it is a first order accurate implicit integration algorithm.

By multiplying eqn (73) by $\Delta t_n (= t_{n+1} - t_n)$:

$$(\Delta\varepsilon_{vp})_{n+1} = \frac{\Delta t_n}{\mu}\underline{C}_e^{-1} : (\underline{\sigma}_{n+1} - \underline{\sigma}^*_{n+1})$$

$$\Delta\underline{q}_{n+1} = -\frac{\Delta t_n}{\mu}(\underline{q}_{n+1} - \underline{q}^*_{n+1}) \tag{74}$$

where the subscript $n+1$ signifies the current time step. Further, the elastic strain is:

$$(\Delta\underline{\varepsilon}_e)_{n+1} = (\Delta\underline{\varepsilon})_{n+1} - (\Delta\underline{\varepsilon}_{vp})_{n+1} = \underline{C}_e^{-1} : (\underline{\sigma}_{n+1} - \underline{\sigma}_n) \tag{75}$$

where $\underline{\sigma}_n$ is the converged stress value at the last time step t_n. By rearranging terms in eqn (74), we obtain the following rate-independent solution:

$$\underline{\sigma}_{n+1} = \frac{[\underline{\sigma}_n + \underline{C}_e : \Delta\underline{\varepsilon}_{n+1}] + \Delta t_n/\mu\, \underline{\sigma}^*_{n+1}}{1 + \Delta t_n/\mu}$$

$$\underline{q}_{n+1} = \frac{\underline{q}_n + \Delta t_n/\mu\, \underline{q}^*_{n+1}}{1 + \Delta t_n/\mu} \tag{76}$$

in which $\underline{q}_n$ is the converged value of $\underline{q}$ from the last time step t_n. It is noted that the term $[\underline{\sigma}_n + \underline{C}_e : \Delta\underline{\varepsilon}_{n+1}]$ is actually the elastic predictor stress $\underline{\sigma}^{(0)}_{n+1}$.

It is observed that $\Delta t_n/\mu$ is the key factor for controlling rate and viscosity effects (see Fig. 2). As $\Delta t_n/\mu$ approaches zero the elastic response is recovered from eqn (76):

$$\underline{\sigma}_{n+1} = \underline{\sigma}^{(0)}_{n+1}, \quad \underline{q}_{n+1} = \underline{q}_n. \tag{77a}$$

On the other hand, as $\Delta t_n/\mu$ approaches infinity the non-viscid plasticity is obtained:

$$\underline{\sigma}_{n+1} = \underline{\sigma}^{*}_{n+1}, \quad \underline{q}_{n+1} = \underline{q}^{*}_{n+1}. \tag{77b}$$

It should be realized that the above integration algorithm is unconditionally stable with respect to the time increment Δt_n. This is certainly favourable in implicit finite element computations. However, it is only a first order accurate algorithm. In order to improve accuracy, the subincremental technique can be used.

It is also noted that, in the above derivation, the Jaumann stress rate modification is not taken into account. In fact it can be involved in the "elastic predictor", that is:

$$\underline{\sigma}_{n+1} = \frac{\underline{\sigma}^{(0)}_{n+1} + \Delta t_n/\mu\, \underline{\sigma}^{*}_{n+1}}{1+\Delta t_n/\mu} \quad \underline{q}_{n+1} = \frac{\underline{q}_n + \Delta t_n/\mu\, \underline{q}^{*}_{n+1}}{1+\Delta t_n/\mu} \tag{78}$$

in which the expressions of $\underline{\sigma}^{(0)}_{n+1}, \underline{\gamma}^{(0)}_{n+1}$ are given in the next section.

5. COMPUTATION ALGORITHM FOR ANISOTROPIC DAMAGE MODEL

5.1. *Transformation between material principal axes and reference axes*

In a nonlinear finite element analysis, the contitutive equations of the material have to be integrated locally at each time step. If stresses, state variables, etc...are expressed in global coordinates, at the beginning of each new step $n+1$, they first be transferred to the principal axes of anisotropy using the classical rules of coordinates transformations. Then, the constitutive relation developed above can be used directly. At the end of the step, the results have to be transferred back to the global coordinates.

5.2. *Operator splitting methodology*

The return mapping algorithm has been used for the integration of elastoplastic constitutive relations. However, the classical integration rule which is in fact particular cases of the trapezoidal and midpoint rule is restricted to the simple plasticity model. For complex models, Simo and Ortiz (1984) proposed a new class of return mapping algorithms with the operator splitting methodology. General elastoplastic behaviour, with plastic hardening or softening, associated or non-associated flow rules and nonlinear elastic response can be efficiently treated with this algorithm. Recently, Benallal and Billardon

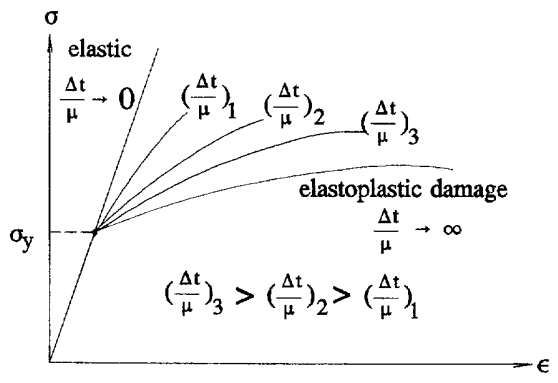

Fig. 2. Range of elasto-viscoplastic behavior.

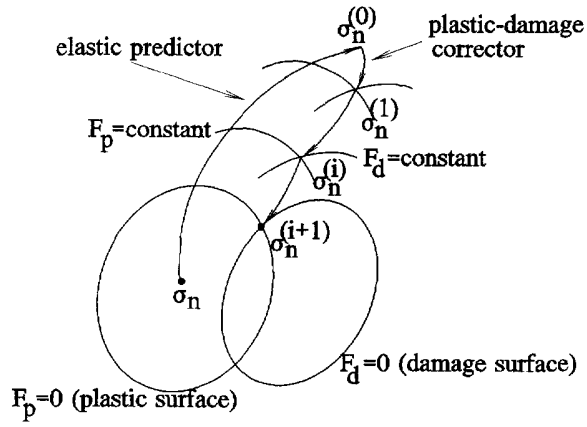

Fig. 3. Elastic predictor/plastic-damage corrector.

(1988), Simo and Ju (1987b) applied this operator splitting methodology to their elastoplastic damage models. Although plasticity and damage are coupled in rate equations, the algorithmic treatments uncouples plasticity and damage, because as soon as the plasticity is corrected, all the damage variables are fixed. In this paper, we propose a fully coupled integration scheme with a two-step (elastic predictor and coupled plastic-damage) corrector. In our model, there exists two coupled surfaces, and for each iteration, the plastic surface and damage surface should be corrected together (see Fig. 3). The computational aspect described in detail can be found in (Zhu, 1992, chapter 6). The different steps of the integration algorithm are detailed below.

5.2.1. *Two step operator split.* The two step operator is shown in Table 2.

5.2.2. *Elastic predictor.* (a) Strain update

$$\Delta\underline{\varepsilon}_{n+1} = \tfrac{1}{2}(\underline{L}+\underline{L}^T)\Delta t_n.$$

(b) Elastic trial stress

Table 2. Operator split

Elastic part	Plastic-damage part
$\dot{\underline{\varepsilon}} = \frac{1}{2}(\underline{L}+\underline{L}^T)$	0
$\dot{\underline{\varepsilon}}_p = 0$	$\dfrac{\underline{M}\,\underline{H}\,\underline{M}\,\underline{\sigma}}{2\bar{\sigma}_F}\dot{\lambda}_p$
$\dot{\alpha} = 0$	$\dot{\lambda}_p$
	$\dfrac{dR}{d\alpha}\dot{\lambda}_p$
$\dot{R} = 0$	
$\dot{\underline{D}} = 0$	$-\dfrac{JY}{2Y_{eq}}\dot{\lambda}_d$
$\dot{\beta} = 0$	$\dot{\lambda}_d$
$\dot{B} = 0$	$\dfrac{dB}{d\beta}\dot{\lambda}_d$
$\dot{\underline{\sigma}} = \underline{M}^{-1}\underline{C}_e\underline{M}^{-1}\dot{\underline{\varepsilon}}+\underline{\Omega}\,\underline{\sigma}'+\underline{\sigma}'\,\underline{\Omega}$	$-\underline{E}^*\dot{\lambda}_p-\underline{F}^*\dot{\lambda}_d$

$$\underline{\sigma}_{n+1}^{(0)} = \underline{\sigma}_n + \underline{M}^{-1}\,\underline{C}_e\,\underline{M}^{-1}\,\Delta\underline{\varepsilon}_{n+1} + \underline{\Omega}_{n+1}\underline{\sigma}'_n\,\Delta t_n - \underline{\sigma}'_n\,\underline{\Omega}_{n+1}\,\Delta t_n \underline{q}_{n+1}^{(0)} = \underline{q}_n.$$

5.2.3. *Plastic-damage corrector.* (c) Check for plastic yield and damage evolution

$$\text{if } (F_p)_{n+1}^{(i)} \leqslant TOL \times R_0 \wedge (F_d)_{n+1}^{(i)} \leqslant TOL \times B_0, \text{ then go to (f)}$$

(d) Plastic-damage return mapping corrector
According to the formulae:

$$(F_p)_{n+1}^{(i)} + \left.\frac{\partial F_p}{\partial \bar{\sigma}}\right]_{n+1}^{(i)} \Delta\bar{\sigma}_{n+1}^{(i)} - \left.\frac{\mathrm{d}R}{\mathrm{d}\alpha}\right]_{n+1}^{(i)} (\Delta\lambda_p)_{n+1}^{(i)} \approx 0 \tag{79}$$

$$(F_d)_{n+1}^{(i)} + \left.\frac{\partial F_d}{\partial \underline{Y}}\right]_{n+1}^{(i)} \Delta\underline{Y}_{n+1}^{(i)} - \left.\frac{\mathrm{d}B}{\mathrm{d}\beta}\right]_{n+1}^{(i)} (\Delta\lambda_d)_{n+1}^{(i)} \approx 0$$

and noting (54), (62), we can obtain:

$$(\Delta\lambda_p)_{n+1}^{(i)} = \frac{a_{22}(F_p)_{n+1}^{(i)} - a_{12}(F_d)_{n+1}^{(i)}}{a_{11}a_{22} - a_{12}a_{21}} \tag{80}$$

$$(\Delta\lambda_d)_{n+1}^{(i)} = \frac{a_{11}(F_d)_{n+1}^{(i)} - a_{21}(F_p)_{n+1}^{(i)}}{a_{11}a_{22} - a_{12}a_{21}}$$

in which:

$$\begin{aligned}
a_{11} &= \frac{\underline{\sigma}\,\underline{M}\,\underline{H}\,\underline{C}^*}{2\bar{\sigma}_F} + \frac{\mathrm{d}R}{\mathrm{d}\alpha} \\
a_{12} &= \frac{\underline{\sigma}\,\underline{M}\,\underline{H}}{2\bar{\sigma}_F}\underline{D}^* \\
a_{21} &= \frac{\underline{Y}\,\underline{J}\,\underline{H}^*}{2Y_{eq}} \\
a_{22} &= \frac{\underline{Y}\,\underline{J}\,\underline{I}^*}{2Y_{eq}} + \frac{\mathrm{d}B}{\mathrm{d}\beta}.
\end{aligned} \tag{81}$$

Computationally, the only modification needed to take account of the anisotropic microcrack opening mechanism for "brittle" damage now is the addition of an eigenvalue calculation to compute the positive (tensile) projection of the stress tensor. Then, the stresses used in $\underline{Y}$, Y_{eq}, a_{12}, a_{21}, a_{22} are replaced by the tensile stresses.
(e) Update stresses and state variables

$$\begin{aligned}
(\underline{\sigma})_{n+1}^{(i+1)} &= (\underline{\sigma})_{n+1}^{(i)} - (\underline{E}^*\Delta\lambda_p)_{n+1}^{(i)} - (\underline{F}^*\Delta\lambda_d)_{n+1}^{(i)} \\
\alpha_{n+1}^{(i+1)} &= \alpha_n^{(i)} + (\Delta\lambda_p)_{n+1}^{(i)} \\
R_{n+1}^{(i+1)} &= R_{n+1}^{(i)} + \left[\frac{\mathrm{d}R}{\mathrm{d}\alpha}\Delta\lambda_p\right]_{n+1}^{(i)} \\
\underline{D}_{n+1}^{(i+1)} &= \underline{D}_{n+1}^{(i)} - \left[\frac{\underline{J}\,\underline{Y}}{2Y_{eq}}\Delta\lambda_d\right]_{n+1}^{(i)} \\
\beta_{n+1}^{i+1} &= \beta_{n+1}^{(i)} + (\Delta\lambda_d)_{n+1}^{(i)}
\end{aligned}$$

$$B_{n+1}^{(i+1)} = B_{n+1}^{(i)} + \left[\frac{\mathrm{d}B}{\mathrm{d}\beta}\Delta\lambda_d\right]_{n+1}^{(i)}.$$

Set up $i \leftarrow i+1$, and go back to (c)

5.3. *Viscous regularization*

(f) Visco-plastic-damage corrector

$$\underline{\sigma}_{n+1} = \frac{\underline{\sigma}_{n+1}^{(0)} + \Delta t_n/\mu\, \underline{\sigma}_{n+1}^{(i+1)}}{1+\Delta t_n/\mu}$$

$$q_{n+1} = \frac{q_{n+1}^{(0)} + \Delta t_n/\mu\, q_{n+1}^{(i+1)}}{1+\Delta t_n/\mu}.$$

5.4. *Evaluation of the incremental compliance matrix $\underline{\mathbf{C}}$ by perturbation technique*

The incremental compliance matrix $\underline{\mathbf{C}}$ can be defined by:

$$\dot{\underline{\sigma}} = \underline{\mathbf{C}}\,\underline{L}. \tag{82}$$

It is well-known that $\underline{\mathbf{C}}$ plays an important part in computing the global stiffness matrix (see chapter 2 of Zhu, 1992). There exist three approaches to evaluate the incremental compliance matrix $\underline{\mathbf{C}}$: the continuum tangent operator, the consistent tangent operator and the numerical perturbation technique.

It was Cescotto and Charlier (1985) who first proposed a numerical perturbation technique to evaluate matrix $\underline{\mathbf{C}}$ for their own elasto-visco-plastic model. Because of its simplicity and its generality, the perturbation technique has been applied to various constitutive laws (Zhu, 1992). Kojic and Bathe (1987) also presented, independently, this approach to compute matrix $\underline{\mathbf{C}}$ for thermo-elasto-plasticity and creep model in ADINA. The main drawback is that the computational cost is slightly more expensive by this approach than by the other two approaches.

The incremental compliance matrix $\underline{\mathbf{C}}$ corresponding to the stress–strain state at the end of the time (loading) step from t_n to t_{n+1}, is defined by:

$$\underline{\mathbf{C}}_{n+1} = \frac{\partial \underline{\sigma}_{n+1}}{\partial(\underline{L}\Delta t)_{n+1}}. \tag{83}$$

The simplest way to compute the above derivative is to use a numerical perturbation technique: each component of $(\underline{L}\Delta t)_{n+1}$ is successively given in a small increment δ and the corresponding increments of $(\tilde{\underline{\sigma}}_{n+1} - \underline{\sigma}_{n+1})$ are computed by the chosen integration scheme. This allows the construction of $\underline{\mathbf{C}}$ column by column. The computational procedure consists of the following steps.

(g) Form the j-th perturbed vector

$$(\tilde{\underline{L}}\Delta t)_{n+1}^{(j)} = (\underline{L}\Delta t)_{n+1} + \delta^{(j)}$$

go to (a) for evaluating $\tilde{\underline{\sigma}}_{n+1}^{(j)}$.

(h) Compute the stress perturbation vector

$$\delta\underline{\sigma}^{(j)} = \tilde{\underline{\sigma}}_{n+1}^{(j)} - \underline{\sigma}_{n+1}.$$

(i) Compute the column vector

$$\underline{\mathbf{C}}^{(j)} = \frac{\delta \underline{\sigma}^{(j)}}{\delta^{(j)}} \quad (\text{no sum on } j).$$

(j) If $j < I$ (I is the dimension of matrix $\underline{\mathbf{C}}$) then set up $j \leftarrow j+1$, go to (g).
(k) Compose matrix $\underline{\mathbf{C}}$

$$\underline{\mathbf{C}}_{n+1} = [\underline{\mathbf{C}}^{(1)}, \underline{\mathbf{C}}^{(2)}, \ldots, \underline{\mathbf{C}}^{(I)}].$$

(l) End of integration of anisotropic constitutive law.

6. NUMERICAL RESULTS AND DISCUSSIONS

The sheet forming processes are widely used in the automotive industry for the production of car body components. In these processes, the forming limit is governed by plastic instability and fracture following the damage growth. Several material aspects may be considered including: initial and induced anisotropy, hardening, softening, temperature, as well as friction between sheet and tools. Good representation of sheet behaviour will be essential to predict and avoid defects (necking, fracture, wrinkling). Hereafter, the present anisotropic damage model is applied to sheet forming simulation. As illustrative examples, hemispherical punch stretching including heat transfer and deep drawing by cylindrical and square punches are simulated.

All the numerical simulations are carried out by mixed finite elements developed in Chapter 4 of (Zhu, 1992). We use the following notations: "BLZ2D-n" denotes the 4-node quadrilateral solid with n-point quadrature; "BLZ3D-n" denotes the 8-node hexahedral solid element with n-point quadrature; "BLZ2T-n" and "BLZ3T-n" are the corresponding thermal–mechanical elements.

6.1. *Non-isothermal hemispherical punch stretching*

This example corresponds to a benchmark test for the numerical simulation of sheet forming processes (Kim and Wagoner, 1991). The current study is aimed at developing a reliable anisotropic damage model and efficient numerical method to solve coupled thermoplasticity and damage problems related to sheet-forming processes. To avoid unnecessary complexity, attention is restricted to temperature-independent material properties. The introduction of temperature dependent material properties, leading to additional coupling terms, does not present fundamental difficulties.

Figure 4(a) shows the geometry of the hemispherical punch and circular die as well as the axisymmetric sheet. The finite element discretization consists of 100 axisymmetric 4-node mixed elements (BLZ2T-2) with 50 along the sheet and two across the thickness. The clamping at the outer perimeter is assumed to be perfect so that the displacements at these nodes are prescribed to be zero. The material properties of the specimen are those listed in Table 3. It is emphasized that the sheet is isotropic in its plane but anisotropic in the thickness direction (direction 2).

The punch and die are isothermal with environmental temperature 298K, the sheet is heated initially to 348K. The heat transfer to tool and air and internal heat conduction in sheet are considered. A constant punch velocity of 40 mm/s is chosen in the whole simulation. The contact problem and heat transfer on the sheet surface are treated by axisymmetric contact elements (Cescotto and Charlier, 1993). The initial and deformed shapes of the sheet are shown in Fig. 4.

The distributions of equivalent stress, damage and temperature for the sheet after a punch displacement of 40 mm are shown in Fig. 5. The punch force versus punch depth is shown in Fig. 6. Figure 7 (a–c) shows the distributions of equivalent stress, strain and damage along the original radial position for a punch depth of 40 mm.

In Figs 5–8, comparison of anisotropy with and without friction is given. Higher punch force is predicted for the anisotropy with friction case. As expected, when the friction

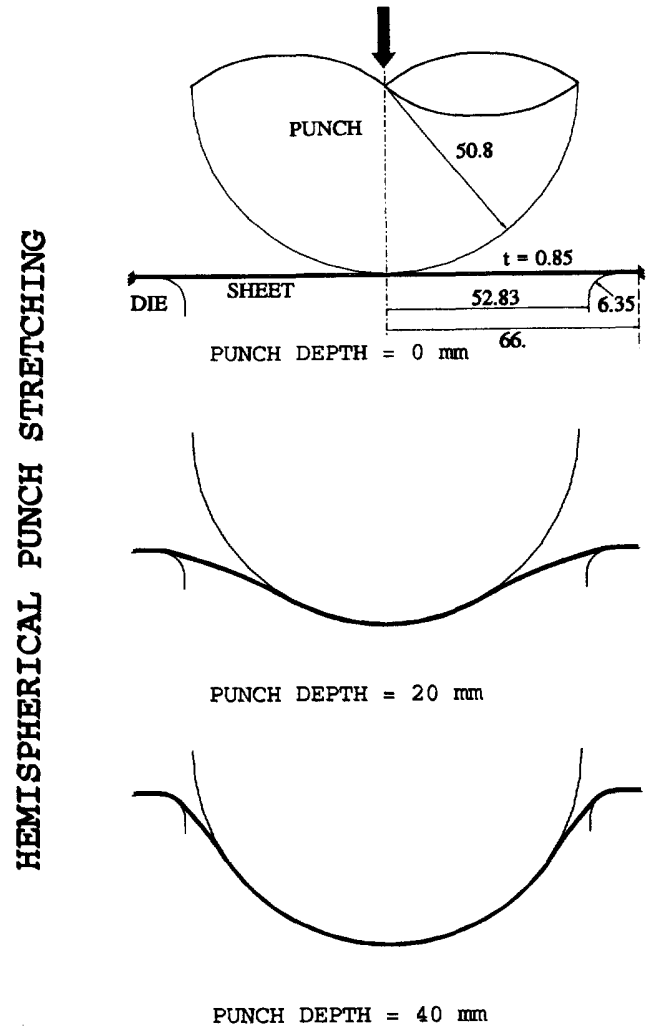

Fig. 4. Initial and deformed configuration.

Table 3. Material properties of sheet

Young's modulus (MPa)	$E_1 = E_2 = E_3 = 2.068 \times 10^5$
Poisson's ratio	$\nu_{12} = \nu_{21} = \nu_{23} = \nu_{32} = \nu_{31} = \nu_{13} = 0.285$
Initial yield stress (MPa)	$\sigma_{1y} = \sigma_{3y} = 170.3$
	$\sigma_{2y} = 170.3$ (for isotropy) 201.5 (for anisotropy)
Elastoplastic tangent modulus (MPa)	$E_{t1} = E_{t3} = 340.4$
	$E_{t2} = 340.4$ (for isotropy) 402.8 (for anisotropy)
	$G_{t12} = G_{y23} = 113.5$
	$G_{t13} = 113.5$ (for isotropy) 134.3 (for anisotropy)
Initial damage energy release rate (MPa)	$Y_{10} = Y_{30} = 0.2$
	$Y_{20} = 0.2$ (for isotropy) 2 (for anisotropy)
Damage hardening (MPa)	$D_{t1} = D_{t3} = 10$
	$D_{t2} = 10$ (for isotropy) 100 (for anisotropy)
Mass density (kg/m^3)	$\rho = 7800$
Thermal expansion coefficient (K^{-1})	$\alpha_1 = \alpha_2 = \alpha_3 = 1.2 \times 10^{-5}$
Taylor-Quinney's coefficient	$\eta = 0.9$
Heat capacity N/(m^2 K)	$\rho\, C_v = 3.77 \times 10^6$
Conductivity N/(S K)	$\lambda_1 = \lambda_2 = \lambda_3 = 36$
Heat radiation coefficient (N/(ms K^4)	$\sigma_r\, \varepsilon_r = 8.5 \times 10^{-9}$
Heat transfer coefficient (N/(ms K)	$h_t = 2.95$
Thermal resistance coefficient (N/(ms K)	$h_r = 4 \times 10^3$
Penalty coefficient (N/m^3)	$K_p = K_t = 1.0 \times 10^{12}$
Coulomb friction coefficient	$\phi = 0$ (without friction) 0.17 (with friction)

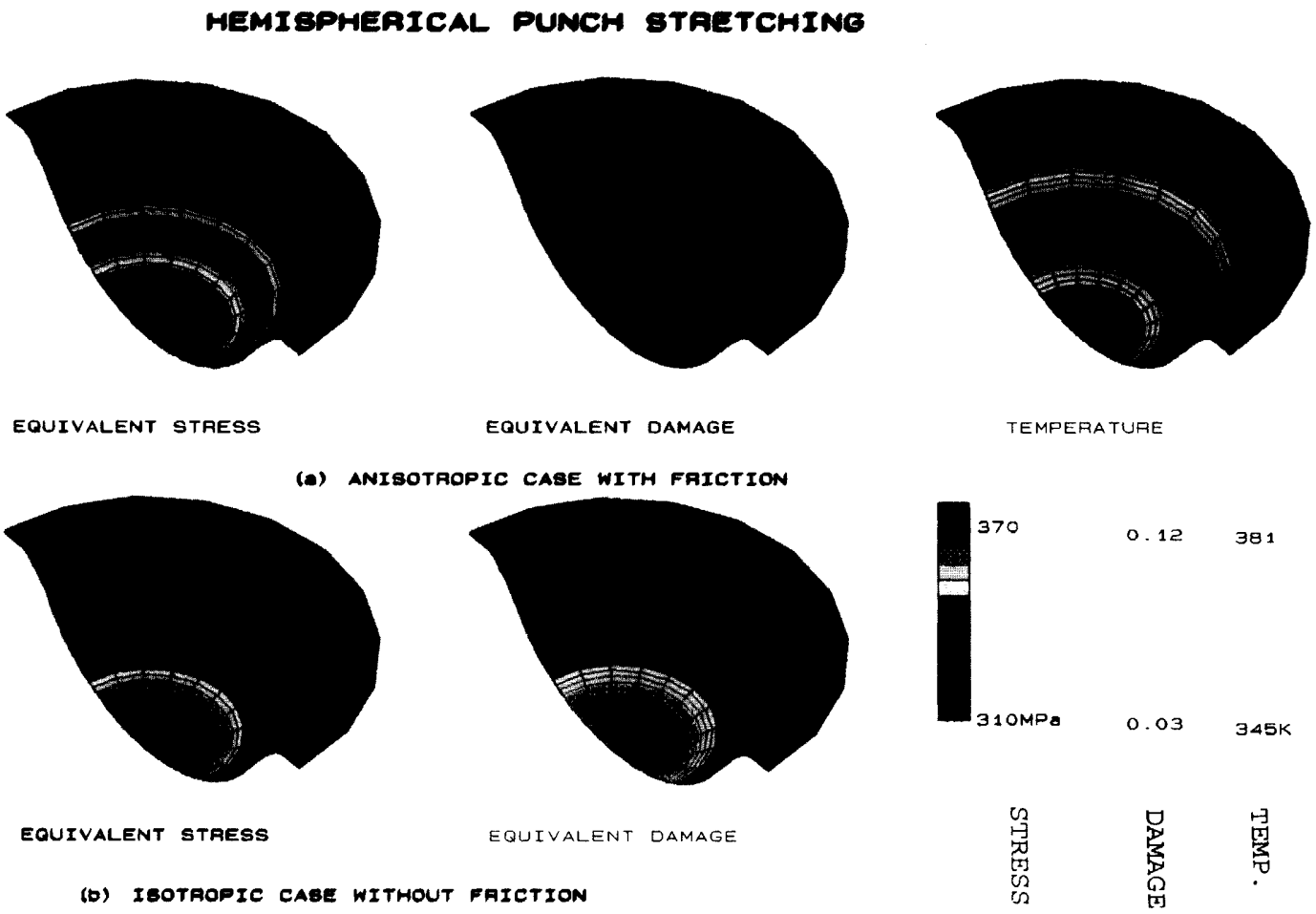

Fig. 5. Distributions for stress, damage and temperature.

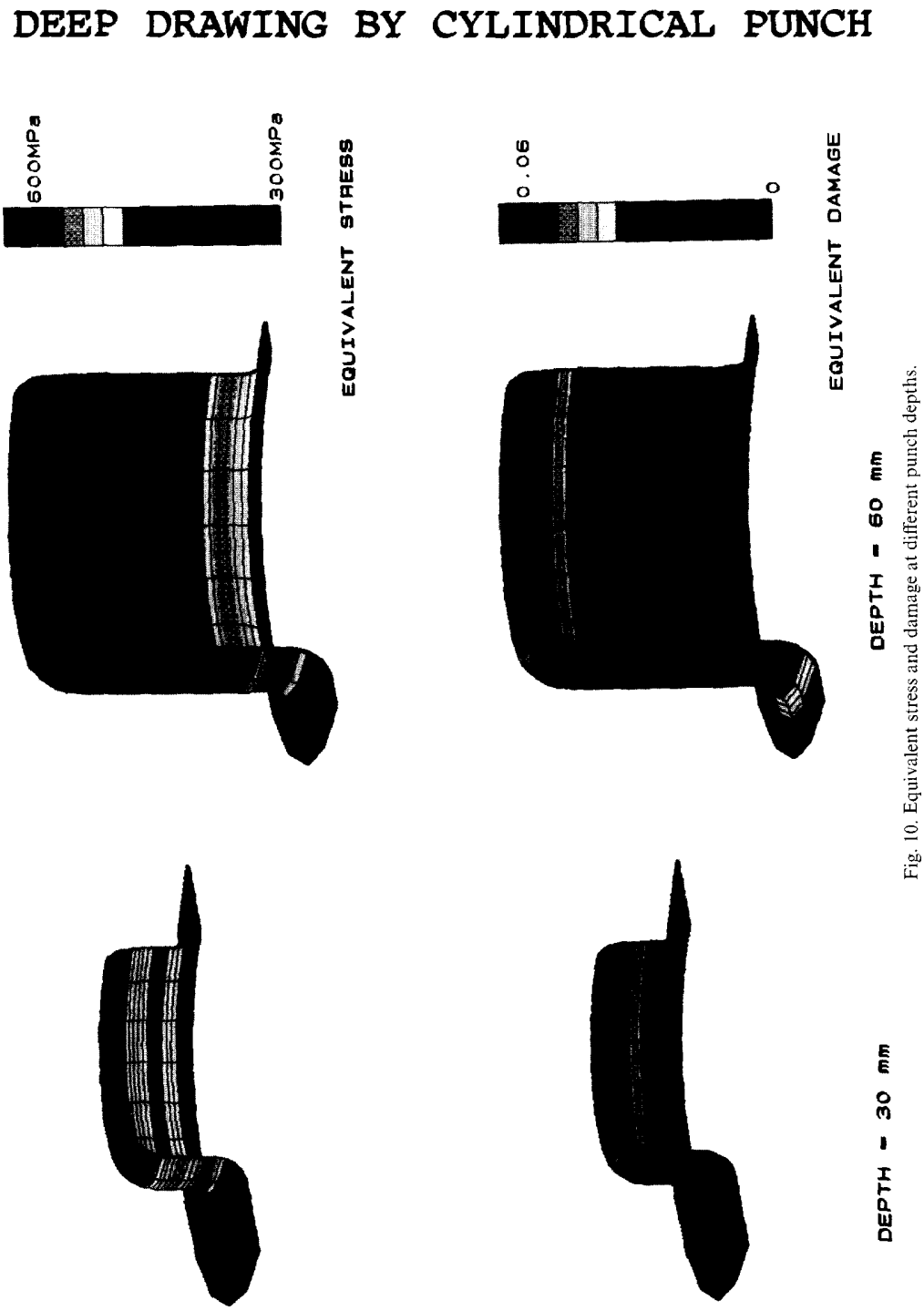

Fig. 10. Equivalent stress and damage at different punch depths.

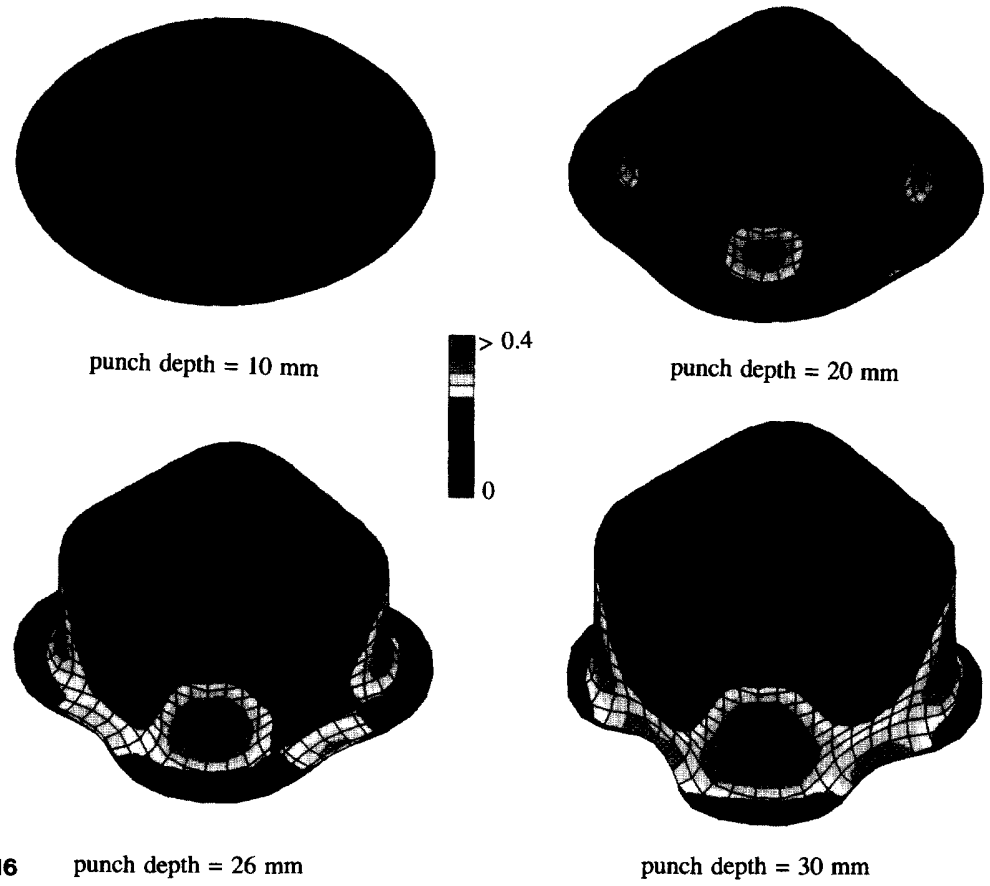

Fig. 16. Deep drawing of a square cup from a circular blank. Distribution patterns of the equivalent plastic strain and deformed configurations.

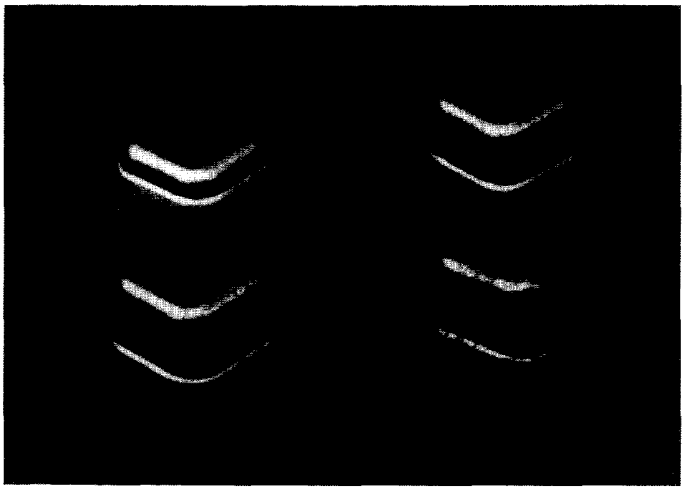

Fig. 17. Photographs of the square cup at different stages of the drawing process.

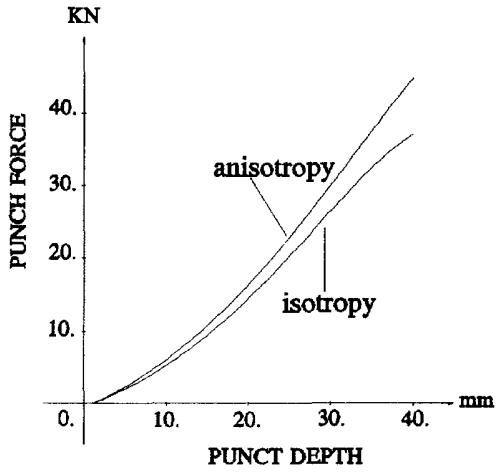

Fig. 6. Punch force versus punch depth.

coefficient increases, the sheet becomes stiffer. In our simulation we find that as the friction between the sheet and tool is decreased or the anisotropy degree is reduced, the peak stress, strain, damage and temperature move towards the center of the sheet and the peak values are increased. In the case of isotropy without friction, the peak values locate near the center of the sheet and the equivalent damage is three times higher than that in the case of anisotropy with friction. Therefore, for sheet metal forming problems, it may be necessary to introduce the effects of initial and current anisotropy.

In Fig. 8, the radial strain distributions along the original radial position are shown for the cases: (a) anisotropy with friction at a punch depth of 40 mm, (b) anisotropy with friction at a punch depth of 35 mm, (c) isotropy without friction at a punch depth of 40 mm. In the same figure, other previous experimental results (Ghosh and Hecker, 1975) and theoretical results (Wang and Budiansky, 1978) are also plotted. These results are relevant to a punch depth between 35 mm and 38 mm. Good agreement can be found between our anisotropic results and other investigator's results.

6.2. *Deep drawing of an axisymmetric cup*

In the deep drawing process the sheet is not fixed at the boundary but is allowed to move between die and blankholder. From a numerical point of view, deep drawing is a more difficult problem to handle than stretch forming because the relative displacements between the sheet and the tools are large. The interaction between sheet, die and blankholder is the most critical aspect of the process. Various aspects of this problem have been treated abundantly in the literature (Saran and Samuelsson, 1990a,b; Garino and Oliver, 1992).

The geometry of this axisymmetric deep drawing by a cylindrical punch is defined in Fig. 9. The material properties of the sheet are listed in Table 4. Normally, deep drawing is performed with a blankholder force of 54.445 kN defined as the total force acting on blankholder and perpendicular to the cup flange. For the sake of simplicity, it was assumed that the distance between blankholder and die is fixed to the initial sheet thickness and the blankholder force is replaced by a radial resistance force of 2.6 kN ($= 2 \times 0.15 \times 54.445/2\pi$) acting on the outer perimeter of the cup flange. The cup flange restrains some of the radial deformation and increases the stretching, but the effects are not major.

The deformed shapes of the cup at various stages of the drawing process are shown in Fig. 10. A uniformly spaced mesh of 50 elements along the sheet and two elements across the thickness is used. Consequently 100 BLZ2D-4 elements are utilized. The resulting cup at a punch depth of 60 mm is depicted in Fig. 9 (for clarity, a partial view is given).

The distributions of equivalent stress and damage at punch depths of 30 mm and 60 mm are shown in Fig. 10. The peak stress appears near the corner of the die (the die contact region); while the higher level of damage locates near the punch corner (the punch contact

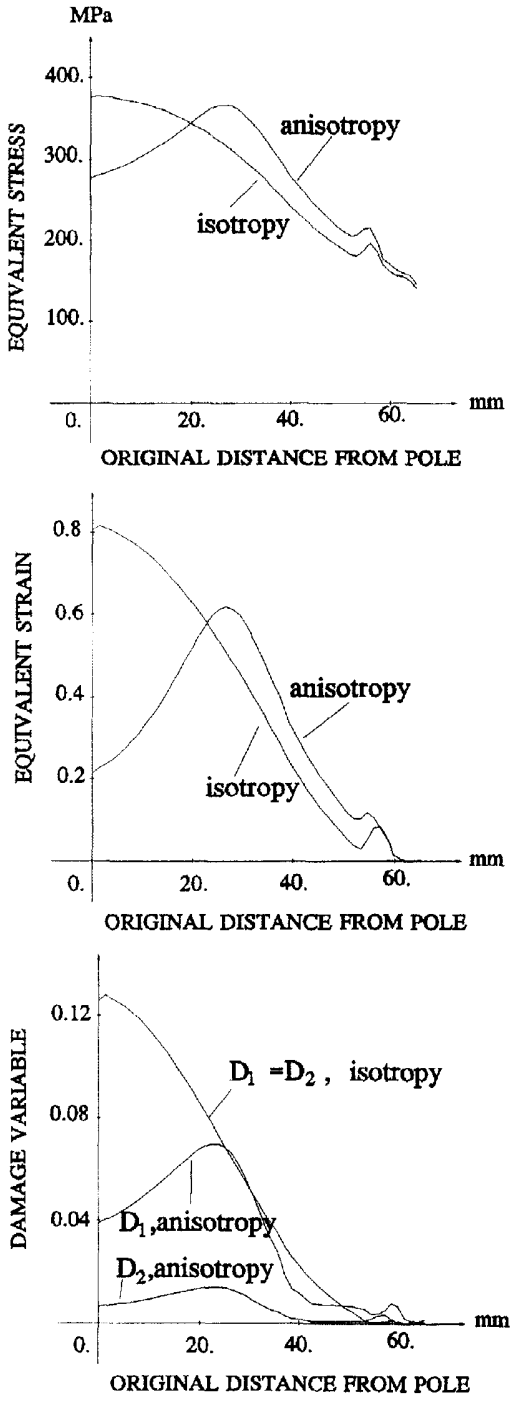

Fig. 7. Radial distribution of quantities along the original radial position for a punch depth of 40 mm.

region) and near the outside bottom of cup. Figure 11 shows the punch force as a function of the punch depth. Three results are given:

(a) theoretical prediction with anisotropic damage model;
(b) theoretical prediction in the case of isotropy;
(c) experimental investigation (Bruneel and De Maré, 1990).

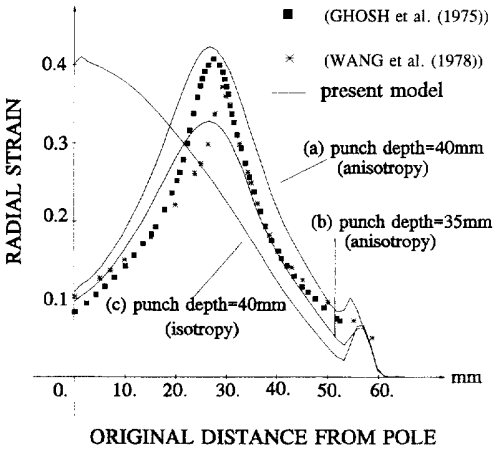

Fig. 8. Distribution of radial strain along the original radial position.

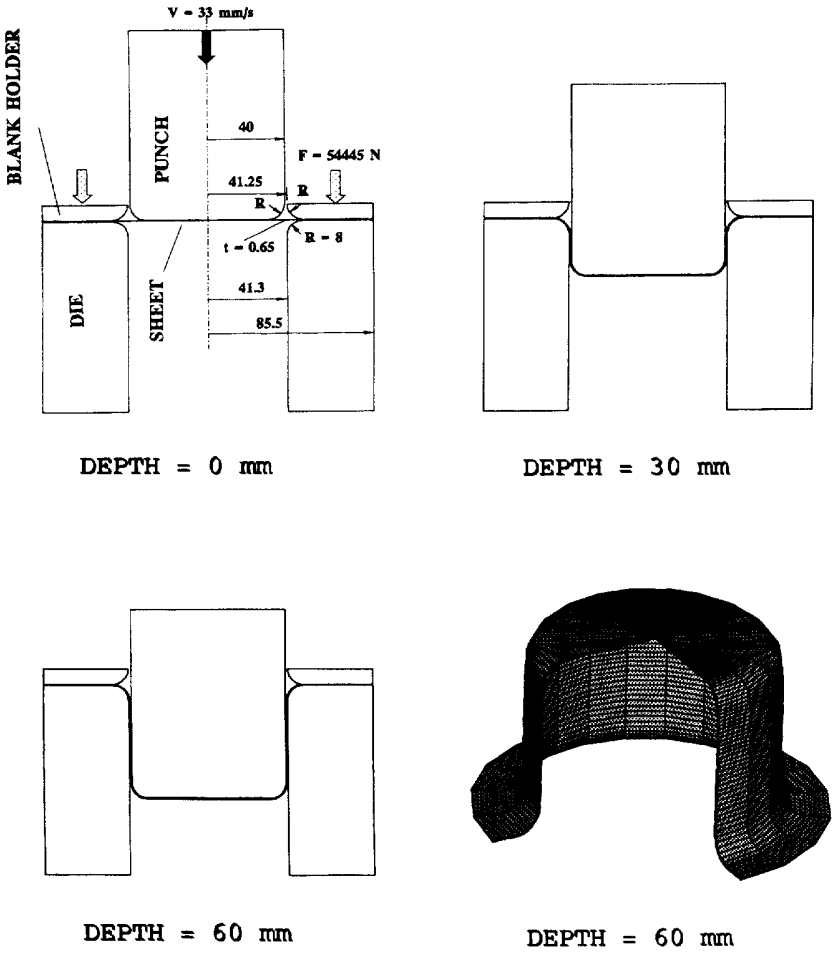

Fig. 9. Initial and deformed sheet shape.

Table 4. Material properties of sheet

Young's modulus (MPa)	$E_1 = E_2 = E_3 = 2.1 \times 10^5$
Poisson's ratio	$\nu_{12} = \nu_{21} = \nu_{23} = \nu_{32} = \nu_{31} = \nu_{13} = 0.3$
Initial yield stress (MPa)	$\sigma_{1y} = \sigma_{3y} = 330.0$
	$\sigma_{2y} = 330.0$ (for isotropy) 495.0 (for anisotropy)
Elastoplastic tangent modulus (MPa)	$E_{t1} = E_{t3} = 210.0$
	$E_{t2} = 210.0$ (for isotropy) 315.0 (for anisotropy)
	$G_{t12} = G_{t23} = 70.0$
	$G_{t13} = 70.0$ (for isotropy) 105.0 (for anisotropy)
Initial damage energy release rate (MPa)	$Y_{10} = Y_{30} = 0.7$
	$Y_{20} = 0.7$ (for isotropy) 2.5 (for anisotropy)
Damage hardening (MPa)	$D_{t1} = D_{t3} = 20.0$
	$D_{t2} = 20.0$ (for isotropy) 100.0 (for anisotropy)
Penalty coefficient (N/m^3)	$K_p = K_\tau = 3 \times 10^{12}$
Coulomb friction coefficient	$\phi = 0.15$

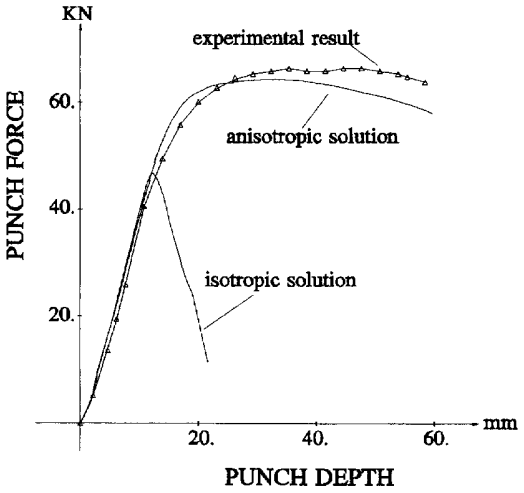

Fig. 11. Comparison of theoretical and experimental results for punch force versus punch depth.

There is good agreement between experimental results and calculations with the anisotropic damage model. However, a necking defect near the punch corner is obtained in the numerical simulation if the material is initially and currently isotropic as shown in Fig. 12. In this case, the punch force drops quickly (Fig. 11), and the numerical simulation looses stability. This necking phenomenon was also encountered by other investigators (Garino and Oliver, 1992).

6.3. *Deep drawing of a square cup from a circular blank*

Deep drawing of a square cup is one of the basic tests among the asymmetrical deep drawing processes and represents typical deformation mechanisms of other similar processes (Kobayashi *et al.*, 1989; Yang *et al.*, 1990; Rebelo *et al.*, 1990; Guo *et al.*, 1990). As a first attempt to handle more complex sheet operations and as a test of the present theories, this case is simulated.

This example is similar to the previous one. The same material and interface (friction) behaviours are used. Figure 13 shows a schematic view of a square cup drawing process. The blank has an original circular shape. The die is fixed and the punch has only vertical displacement with a constant velocity. Deep drawing is performed by imposing prescribed blankholder forces, which are perpendicular to the cup flange and allow thickening of the sheet. The vertical displacement of the blankholder is controlled by vertical equilibrium. The interaction of tools (punch, die, blankholder) with the sheet is crucial to the deep drawing process, since the friction conditions have a strong influence on the material flow, the load in the walls and the punch force.

The material and process variables used in the simulation are listed in Table 5.

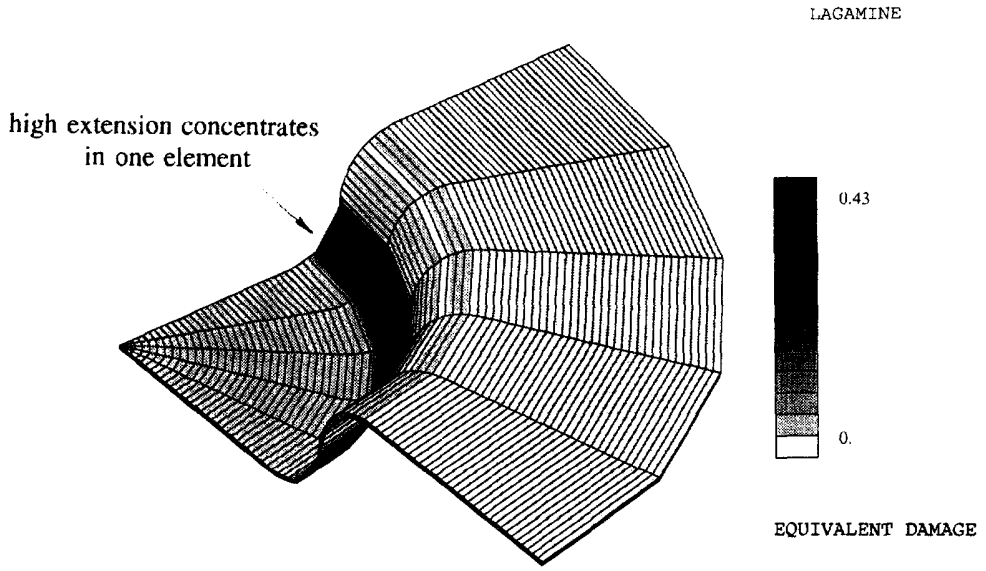

Fig. 12. Necking defect with isotropic model.

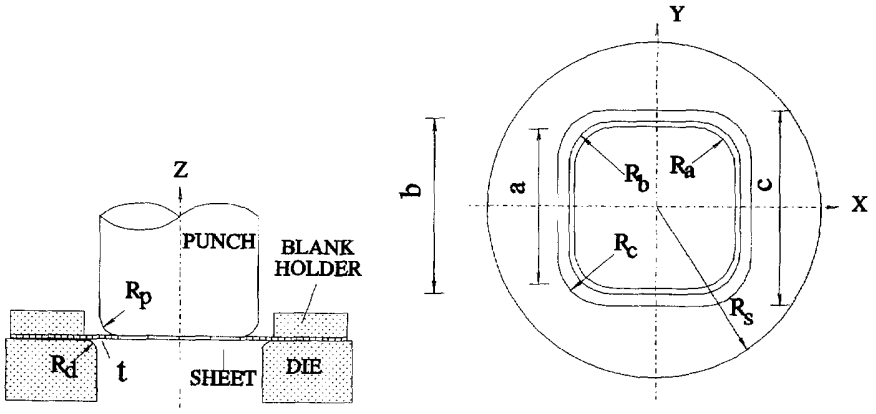

Fig. 13. Schematic view of square cup drawing.

Table 5. The material and process variables

Initial radius of sheet blank R_s	42.5 mm
Initial sheet thickness t	0.8 mm
Punch size a	40×40 mm
Punch radius R_p	4.5 mm
Punch corner radius R_a	10 mm
Die opening b	41.92×41.92 mm
Die radius R_d	3 mm
Die corner radius R_b	10.96 mm
Blankholder opening c	41.3×41.3 mm
Blankholder radius R_s	42.5 mm
Blankholder corner radius R_c	11 mm
Punch vertical velocity V_p	1 mm/s
Blankholding force P	10 KN
Penalty coefficient K_p, K_τ	3×10^{11} N/m^3
Friction coefficient ϕ	0.15

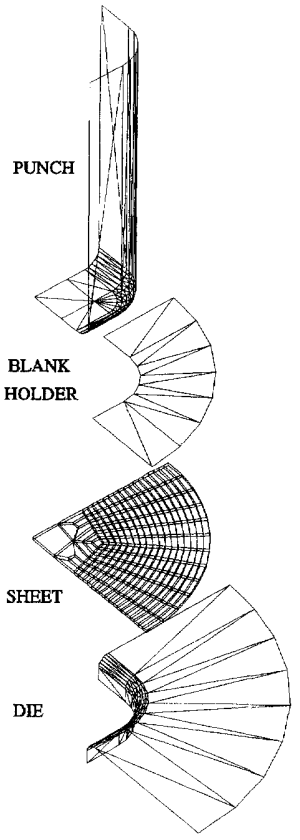

Fig. 14. FEM meshes of sheet and tools.

The analysis proceeds in two steps, corresponding to the phases of the deep drawing process itself. First, a force of 10 kN is applied to the blankholder. This force creates an initial pressure distribution between blankholder, sheet and die. Next the punch is moved to a total depth of 30 mm. Near a punch depth of 25 mm, the load on the blankholder is removed to demonstrate the unloading procedure.

The FEM meshes that are used in the square cup drawing simulation are shown in Fig. 14. Owing to symmetry only one quarter is modelled. The tools are discritized by triangular rigid elements and the sheet is modelled by 218 BLZ3D-8 mixed elements. One element through the thickness is used.

Clearly, during the sheet forming process both sides of the sheet will be in contact with the tools. Sometimes, there is a severe gradient of stress throughout the thickness of the material. On one side of the thickness the stress is tension and on the other side it is either compression or a reduced level of tension (Kobayashi *et al.*, 1989). The URI (uniform reduced integration) scheme 3D solid elements with one layer through the thickness and even some kinds of shell element are unable to simulate this accurately, because they cannot accommodate the thickness stress (Rebelo *et al.*, 1990; Wertheimer, 1991). For inelastic calculations, we know that more integration points through the thickness provide a more accurate solution. An economical treatment in this case is to use a single layer of solid elements with hourglass and locking controls—BLZ3D-4 and BLZ3D-8, which have been developed in Chapter 4 of (Zhu, 1992), including good shear and bending behaviours. These provide the advantages of some shell elements and are directly applicable to two-surface contact conditions. Here, the results of BLZ3D-8 are given.

The punch force over the punch depth is shown in Fig. 15. Figure 16 shows distribution patterns of the equivalent plastic strain and deformed mesh configurations at various stages of the drawing process. It can be seen that for the square cup, the maximum equivalent

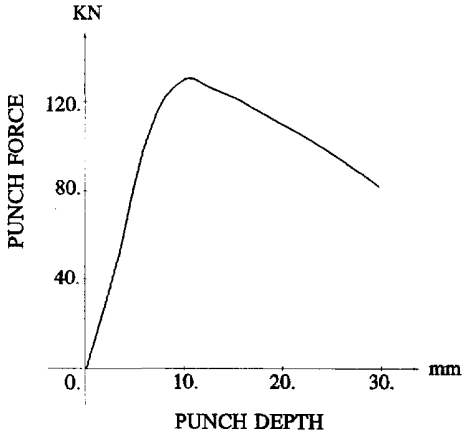

Fig. 15. Punch force over punch depth.

plastic strain in particular is concentrated at the corner wall near the die shoulder. This is the place where failure is most likely to occur.

In Fig. 17, photographs of the square cup at different stages of the drawing process are shown. The crack appears at the corner of the cup. This confirms the theoretical prediction.

7. CONCLUSIONS

An energy-based anisotropic elasto-visco-plastic damage model at finite strain has been presented in this paper to characterize progressive damage and crack growth. The constitutive model is developed within the general framework of continuum thermodynamics for irreversible processes by identifying a proper set of internal variables together with their conjugate generalized forces. The proposed framework is capable of accommodating general nonlinear elastoplastic response, the coupling of damage and plasticity, damage threshold, anisotropic microcrack opening and closing. The evolution laws of anisotropic damage are developed by adopting the damage surface concept as well as the principle of maximum damage dissipation. The material anisotropy is considered for elastic, plastic and damage response: in the elastic regime, by introducing the appropriate elastic constants in the elastic compliance matrix; in plasticity by using material anisotropy parameters in Hill's yield function; in the damage regime, by introducing a new damage characteristic tensor $\underline{J}$ in the damage evolution law, which can be conveniently determined by equivalence of damage work. Throughout the discussion, the concept of energy plays a very important role not only in deriving the damage effect tensor $\underline{M}(\underline{D})$, the damage characteristic tensor $\underline{J}$ and the effective plastic characteristic tensor $\underline{H}$, but also in establishing the plastic evolution law and the damage evolution law.

Another essential purpose of the present work is to demonstrate that the anisotropic damage model is suitable for large-scale computation. In particular, use of the operator splitting methodology leads to a two-step integration algorithm including an elastic predictor and a coupled plastic-damage corrector. Thus the developed model of anisotropic damage growth can be easily implemented in existing finite element programs to solve practical engineering problems.

Numerical examples are also given to illustrate the potential applicability of the proposed model, such as a typical industrial application of sheet metal forming. Comparison of results for isotropic and anisotropic situations illustrates significant differences in structural response. Thus in sheet forming problems where anisotropic conditions are invariably encountered, it is essential to adopt the anisotropic damage model.

Acknowledgements—The authors would like to acknowledge Drs T. Zacharia and S. Šimunović of Oak Ridge National Laboratory for reviewing the manuscript. The research was sponsored in part by the Division of

Materials Sciences, U.S. Department of Energy, under contract DE-AC05-84OR21400 with Martin Marietta Energy System, Inc.

REFERENCES

Benallal, A., Billardon, R. and Doghri, I. (1988). An integration algorithm and the corresponding consistent tangent operator for fully coupled elastoplastic and damaged equations. *Commun. Appl. Numer. Meth.* **4,** 731–740.

Benallal, A., Billardon, R. and Lemaitre, J. (1991). Continuum damage mechanics and local approach to fracture: numerical procedures. *Comp. Meth. Appl. Mech. Engng* **92,** 141–155.

Bruneel, H. and De Maré, C. (1990). Vergelijkende test van FEM-pakketten voor dieptrekken, *CaDM/9030/not, c/o SIDMAR*, Belgium.

Cescotto, S. and Charlier, R. (1985). Numerical simulation of elastic-visco-plastic large strains of metal at high temperature. *Proc. Int. Conf. of Structural Mechanics in Reactor Technology*, Brussels.

Cescotto S. and Charlier R. (1993). Variational principles for mixed contact elements. *Int. J. Numero. Meth. Engng* **36,** 1681–1702.

Chaboche, J. L. (1981). Continuous damage mechanics—a tool to describe phenomena before crack initiation. *Nucl. Engng Des.* **64,** 233 247.

Chaboche, J. L. (1984). Anisotropic creep damage in the framework of continuum damage mechanics. *Nucl. Engng Des.* **79,** 309–319.

Chaboche J. L. (1987). Continuum damage mechanics: present states and future trends. *Nucl. Engng Des.* **105,** 19–33.

Chow, C. L. and Lu, T. J. (1989a). On evolution laws of anisotropic damage. *Engng Fract. Mech.* **34,** 679–701.

Chow, C. L. and Lu, T. J. (1989b). A normative representation of stress and strain for continuum damage mechanics. *J. Theory Appl. Fract. Mech.* **12,** 161–187.

Chow, C. L. and Wang, J. (1987). An anisotropic theory of elasticity for continuum damage mechanics. *Int. J. Fract.* **33,** 3–16.

Chow, C. L. and Wang, J. (1988). Ductile fracture characterization with an anisotropic continuum damage theory. *Engng Fract. Mech.* **30,** 547–563.

Chow, C. L. and Wang, J. (1991). A continuum damage mechanics model for crack initiation in mixed model ductile fracture. *Int. J. Fract.* **47,** 145–160.

Cordebois, J. P. (1983). Critères d'instabilité plastique et endommagement ductile en grandes déformations, application à l'emboutissage. Thèse de Docteur Science Physiques, Université Paris 6.

Cordebois, J. P. and Sidoroff, F. (1979). Damage induced elastic anistropy. Euromech 115, Villard de Lans.

Cordebois, J. P. and Sidoroff, F. (1982). Endommagement anistope en élasticité et plasticité. *J. Méc. Thé. App.*, Numéro spécial, 45–60.

Duvant, G. and Lions, J. L. (1972). *Les Inéquations en Mécanique et en Physique*. Dunod, Paris.

Garino, C. G. and Oliver, J. (1992). Simulation of sheet metal forming using a frictional finite strain elastoplatic model. In *Numerical Methods in Engineering* '92 (Edited by C. Hirsch *et al.*), pp. 185–192. Elsevier, Amsterdam.

Ghosh, A. K. and Hecker, S. S. (1975). Failure in thin sheets stretched over rigid punches. *Metall. Trans.* **6A,** 1065–1074.

Guo, Y. Q. and Batoz, J. L. (1990). Finite element procedures for strain estimations of sheet metal forming parts. *Int. J. Numero. Meth. Engng* **30,** 1385–1401.

Hill, R. (1950). *The Mathematic Theory of Plasticity*. Oxford.

Ju, J. W. (1989a). On energy-based coupled elastoplastic damage theories: constitutive modeling and computational aspects. *Int. J. Solids Structures* **25,** 803–833.

Ju, J. W. (1989b). Energy-based coupled elastoplastic damage models at finite strain. *J. Engng Mech ASCE* **115,** 2507–2525.

Ju, J. W. (1990a). Consistent tangent moduli for a class of viscoplasticity. *J. Engng Mech., ASCE* **116,** 1764–1779.

Ju, J. W. (1990b). Isotropic and anisotropic damage variables in continuum damage mechanics. *J. Engng Mech., ASCE* **116,** 2764–2770.

Jubran, J. S. and Cofer, W. F. (1991). Ultimate strength analysis of structural components using the continuum damage mechanics approach. *Comp. Struct.* **39,** 741–752.

Kim, Y. H. and Wagoner, R. H. (1991). A 3D finite element method for non-isothermal sheet-forming processes. *Int. J. Mech. Sci.* **33,** 911–925.

Kobayashi, S., Oh, S. I. and Altan, T. (1989). *Metal Forming and the Finite Element Method*. New York, Oxford.

Kojic, M. and Bathe, K. J. (1987). The effective-stress-function algorithm for thermo-elasto-plasticity and creep. *Int. J. Numero. Meth. Engng* **24,** 1509–1532.

Lee, H., Peng, K. E. and Wang, J. (1985). An anisotropic damage criterion for deformation instability and its application to forming limit analysis of metal plates. *Engng Fract. Mech.* **21,** 1031–1054.

Lemaitre, J. (1985). A continuous damage mechanics model for ductile fracture. *J. Engng. Mater. & Tech.* **107,** 83–89.

Lemaitre, J. and Chaboche, J. L. (1985). *Mécanque des Matériaux Solids*. Dunod, Paris.

Loret, B. and Prevost, J. H. (1990). Dynamic strain localization in elasto-(visco-)plastic solids, part 1. General formulation and one-dimensional examples. *Comput. Meth. Appl. Mech. Engng* **83,** 247–273.

Lu, T. J. and Chow, C. L. (1990). On constitutive equations of inelastic solids with anisotropic damage. *J. Theory Appl. Fract. Mech.* **14,** 187–218.

Ortiz, M. (1985). A constitutive theroy for the inelastic behavior of concrete. *Mech. Mater.* **4,** 67–93.

Perzyna, P. (1971). Thermodynamic theory of viscoplasticity. In *Advances in Applied Mechanics* Vol. 11, Academic Press, New York.

Prevost, J. H. and Loret, B. (1990). Dynamic strain localization in elasto-(visco-)plastic solids, part 2. Plane strain examples. *Comput Meth. Appl. Mech. Engng* **83,** 275–294.

Rebelo, N., Nagtegaal, J. C. and Hibbit, H. D. (1990). Finite element analysis of sheet forming processes. *Int. J. Numero. Meth. Engng* **30,** 1739–1758.

Saaouni, K. Chaboche, J. L. and Lesne P. M. (1989). On the creep crack-growth prediction by a non-local damage formulation. *Eur. J. Mech.* **8,** 437–459.

Saran, M. J. and Samuelsson, A. (1990a). Numerical and experimental investigations of deep drawing of metal sheets. *J. Engng Ind. ASME.* **112,** 272–277, 1990.

Saran, M. J. and Samuelsson, A. (1990b). Elastic–viscoplastic implicit formulation for finite element simulation of complex sheet forming processes. *Int. J. Numero. Meth. Engng* **30,** 1675–1697.

Simo, J. C. and Ju, J. W. (1987a). Strain and stress-based continuum damage models—I. Formulation. *Int. J. Solids Structures* **23,** 821–840.

Simo, J. C. and Ju, J. W. (1987b). Strain and stress-based continuum damage models—II. Computational aspects. *Int. J. Solids Structures* **23,** 841–869.

Simo, J. C. Kennedy, J. G. and Govindjee, S. (1988). Non-smooth multisurface plasticity and viscoplasticity loading/unloading conditions and numerical algorithms. *Int. J. Numero. Meth. Engng* **26,** 2161–2185.

Simo, J. C. and Ortiz, M. (1984). A unified approach to finite deformation elastoplastic analysis based on the use of hyperelastic constitutive equations. *Comput. Meth. Appl. Mech. Engng* **49,** 221–245.

Valliappan, S., Boonlaulohr, P. and Lee, I. K. (1976). Non-linear analysis for anisotropic materials. *Int. J. Numero. Meth. Engng* **10,** 597–606.

Valliappan, S., Murti, V. and Zhang W. H. (1990). Finite element analysis of anistropic damage mechanics problems. *Engng Fract. Mech.* **35,** 1061–1071.

Voyiadjis, G. Z. and Katton, P. I. (1990). A coupled theory of damage mechanics and finite elastoplasticity—II, damage and finite strain plasticity. *Int. J. Engng Sci.* **28,** 505–524.

Voyiadjis, G. Z. and Katton, P. I. (1992). Finite strain plasticity and damage in constitutive modeling of metals with spin tensor. *Appl. Mech. Rev.* **45,** S92–S109.

Wang, N. M. and Budiansky, B. (1978). Analysis of sheet metal stamping by a finite element method. *J. Appl. Mech.* **45,** 73–82.

Wertheimer, T. (1991). Numerical simulation of metal sheet forming processes. VDI Berichte no. 984, 517–548.

Yang, D. Y., Chung, W. J. and Shim, H. B. (1990). Rigid–plastic finite element analysis of sheet metal forming processes with initial guess generation. *Int. J. Mech. Sci.* **32,** 687–708.

Zhu, Y. Y. and Cescotto, S. (1992). Unified viscoplactic models for dynamic material behavior at high strain rate. Rapport MSM., Université de Liège, 1992.

Zhu, Y. Y. (1992). Contribution to the local approach of fracture in solid dynamics. Doctoral thesis, Liège University, December.